Naval Research Laboratory

Washington, DC 20375-5320

NRL/MR/6110--99-8370

Report on the Characterization of Calspan's 600 m^3 Chamber in Preparation for the NOPP Aerosol Processes Experiments

WILLIAM HOPPEL
GLENDON FRICK
PETER CAFFREY

Remote Sensing Physics Branch
Remote Sensing Division

LOUISE PASTERNACK

Chemistry Dynamics and Diagnostics Branch
Chemistry Division

THOMAS ALBRECHCINSKI
JOHN R. AMBRUSKO
WILLAIM SULLIVAN

Calspan-University of Buffalo Research Center

DEAN HEGG
SONG GAO

University of Washington

April 22, 1999

REPORT DOCUMENTATION PAGE

Form Approved
OMB No. 0704-0188

1. AGENCY USE ONLY (*Leave Blank*)	2. REPORT DATE	3. REPORT TYPE AND DATES COVERED
	April 22, 1999	

4. TITLE AND SUBTITLE

Report on the Characterization of Calspan's 600 m^3 Chamber in Preparation for the NOPP Aerosol Processes Experiments

5. FUNDING NUMBERS

PE - 61153N
BE - 033-02-4K

6. AUTHOR(S)

W. Hoppel, G. Frick, P. Caffrey, L. Pasternack,* T. Albrecheinski,† J.R. Ambrusko,† W. Sullivan,† D. Hegg,‡ and S. Gao‡

7. PERFORMING ORGANIZATION NAME(S) AND ADDRESS(ES)

Naval Research Laboratory
Washington, DC 20375-5320

8. PERFORMING ORGANIZATION REPORT NUMBER

NRL/MR/6110--99-8370

9. SPONSORING/MONITORING AGENCY NAME(S) AND ADDRESS(ES)

Chief of Naval Research
Arlington, VA 22217

10. SPONSORING/MONITORING AGENCY REPORT NUMBER

11. SUPPLEMENTARY NOTES

*Chemistry Division
†Calspan-University of Buffalo, Department of Astrospheric Sciences
‡University of Washington, Department of Chemistry

12a. DISTRIBUTION/AVAILABILITY STATEMENT

Approved for public release; distribution unlimited.

12b. DISTRIBUTION CODE

A

13. ABSTRACT (*Maximum 200 words*)

Calspan's 600 m^3 chamber was characterized in preparation for the National Oceanographic Participation Program (NOPP) Aerosol Processes Experiments. Both physical and chemical measurements were made to test the functioning of the chamber for nucleation and cloud processing experiments.

14. SUBJECT TERMS

Aerosols
Cloud-processing
Nucleation

15. NUMBER OF PAGES

63

16. PRICE CODE

17. SECURITY CLASSIFICATION OF REPORT	18. SECURITY CLASSIFICATION OF THIS PAGE	19. SECURITY CLASSIFICATION OF ABSTRACT	20. LIMITATION OF ABSTRACT
UNCLASSIFIED	UNCLASSIFIED	UNCLASSIFIED	UL

NSN 7540-01-280-5500

Standard Form 298 (Rev. 2-89)
Prescribed by ANSI Std 239-18
298-102

CONTENTS

EXECUTIVE SUMMARY

Calspan's 600 m^3 chamber was characterized in preparation for the National Oceanographic Participation Program (NOPP) Aerosol Processes Experiments. Both physical and chemical measurements were made to test the functioning of the chamber for nucleation and cloud processing experiments.

The chamber is pressurized and then the gas is rapidly expanded to create clouds. To test the operation of the chamber, tests were performed on the pressurization system, the washing and humidification system, and the filtering system. A recommendation was made to reduce the leakage of air from the chamber. The chamber also contains various lamps for photolysis experiments, and their spectral output was measured. The output from these lamps was found to be low in the ultraviolet region needed to photolyze O_3 and ways to improve on the irradiation system were discussed. The system for measuring the liquid water content in the chamber was also tested.

Measurement was made of the background contaminants in the chamber. The background hydrocarbons and the aerosol concentration in the clean chamber were measured. The effects of added O_3 or SO_2 and the effect of photolysis on aerosol production were also determined. It was determined that much of the background aerosols came from the introduction of unfiltered air into the chamber to make up for the amount removed by the investigators for their measurements. A recommendation to add make-up air through aerosol and charcoal filters was made.

Determinations of wall losses in the clean chamber were made for O_3, SO_2, cyclohexene, alpha-pinene, dimethyl sulfide, and aerosols. These measurements also provided tests of the monitoring methods for these compounds. In addition to the wall loss measurements, preliminary studies were made of the aerosol formation caused by the reaction of the hydrocarbons with O_3. Also, preliminary measurements were made of the particle formation due to the reaction of dimethyl sulfide and O_3 both with and without photolysis.

Since some of the proposed NOPP experiments are on the heterogeneous reactions of SO_2 with sea salt aerosols, the method of introducing the sea salt was also tested. Two nebulizers that introduce the sea salt by nebulizing seawater were used. The size distributions of the resulting particles were measured. Preliminary experiments were performed on the reaction of SO_2 and O_3 with the sea salt aerosols.

Cloud processing experiments were conducted to test the cloud processing procedures and the chamber capabilities. These experiments also tested the techniques used for the introduction of reactions and the capability of monitoring equipment. These experiments require the coordination of a large number of simultaneous physical and chemical measurement systems. Measurements were made of the growth of sulfuric acid seed nuclei from gas-phase reaction products, SO_2 oxidation by ozone and hydrogen peroxide during cloud processing, and the cloud processing of hydrocarbons.

As a result of these experiments, specific recommendations were made to improve the physical operation of the chamber. Operating parameters for the reagent handling and measurement systems were obtained. Also, the specific requirements for what measurements will be necessary to fully characterize each of the different types of experiments were determined.

REPORT ON THE CHARACTERIZATION OF CALSPAN'S 600 m^3 CHAMBER IN PREPARATION FOR THE NOPP AEROSOL PROCESSES EXPERIMENTS

I. PHYSICAL CHARACTERISTICS OF THE CHAMBER

Physical Dimensions of the Chamber

Diameter: 9.1 m (30 ft)
Height: 9.1 m (30 ft)
Volume: 590 m^3
Surface area: 394 m^2
Steel walls: 0.5 inches thick
Inside covered with Teflon coating

Chamber Pressurization and Expansion, Fog Cycles

The chamber can be pressurized and expanded to create clouds. Initially the chamber is pressurized by pulling air in through the charcoal filter bank and into the chamber. Manipulating a blower damper controls the rate of pressurization. The chamber can be pressurized to a maximum of 25 mbar, which can be accurately controlled and held at ± 0.5 mbar. The pressure limitation is dictated by the strength of the windows covering the irradiation lamps. During the characterization experiments leaks in ducting and valves resulted in an over-pressure decay time of about 5 minutes; i.e., after over-pressuring, the chamber pressure fell to e^{-1} the maximum value in 5 minutes when the over-pressure blower was turned off. While this is adequate for our cloud processing experiments, improving the sealing would improve the cloud processing performance as discussed in Section V.

Washing and Humidification System

Chamber Humidification

The chamber is equipped with a wall-wetting ring located along the top circumference of the chamber. Deionized water is supplied to the ring by a high-pressure pump. Wetting the walls in two intervals of 3 minutes over a 30 minute period can elevate the chamber relative humidity (RH) to over 97%.

Chamber Dehumidification

The chamber has two copper finned dehumidification coils. These are capable of reducing the relative humidity in the chamber from 100% to < 35% when operated over a 12 hour interval. Lower RH values can be achieved with longer cycle time.

Manuscript approved March 23, 1999

Chamber Wash System

Wash water for the chamber is processed through a filtered deionizing system. Tap water is passed through a 5 μm filter into a charcoal filter bed. It then passes through two resin beds and finally through a 5 μm filter before being transferred to a 300 gallon holding reservoir. The chamber is equipped with an automated pneumatic articulating spray nozzle mounted from the center of the ceiling. When in operation, the entire chamber can be wetted by the spray nozzle every 6 minutes. A thorough wash is accomplished by spraying the chamber interior with a mild soap solution followed by two rinse cycles using deionized water. Each wash and rinse cycle consume approximately 50 gallons of water. The chamber is typically put through a fresh water rinse at the end of each day of operation.

Filtering and Air Purification System

The 600 m^3 chamber facility incorporates a system of pre- and absolute filters to permit virtually the total removal of particulates. Impregnated charcoal filter panels enable the removal of gaseous contaminants. Some of the most difficult to remove contaminants, such as CO and CH_4, are present only at minimum concentrations in the unpurified ambient air due to the rural location of the test facility. The air purification system is thus capable of preconditioning the chamber for studies of tropospheric pollutant and aerosols even at minute concentrations. The chamber "air" system can be operated in various modes depending on the nature of the investigation.

Fresh Air Flush

In this operating mode chamber air is exhausted outdoors via an exhaust blower. Makeup air is supplied through a Farr 30/30 pre-filter followed by a 95%, efficient Ashrae filter.

Charcoal (Absolute) Filtering

In this operating mode chamber air is circulated through a copper finned dehumidifier coil and downstream through a HEPA filter bank. The air then passes through a 30/30 pre-filter and a 95% Ashrae filter followed by a series of two absolute charcoal filters. Finally the air is circulated through a HEPA filter before being returned to the chamber. This is a closed cycle configuration.

Filtering reduces the concentration in half about every 10 minutes for substances that are removed with about 100% efficiency with the filters. This is shown for the total aerosol concentration in Fig. 1.

Characterization of the Chamber Irradiation System

The spectral irradiance characteristics of the 600 m^3 chamber lamp system were determined by direct measurement using a calibrated optical multi-channel analyzer (OMA) along with photolysis of NO_2 to determine total chamber UV intensity.

The chamber contains 3 types of lamps:

1. Very high output (VHO), 96" F96T12 Sylvania, 2 lamps per enclosure
2. High output (HO), 72" F72T12 GE black lamps, 8 lamps per enclosure
3. FS40, 40" Westinghouse sunlamps, 2 lamps per enclosure.

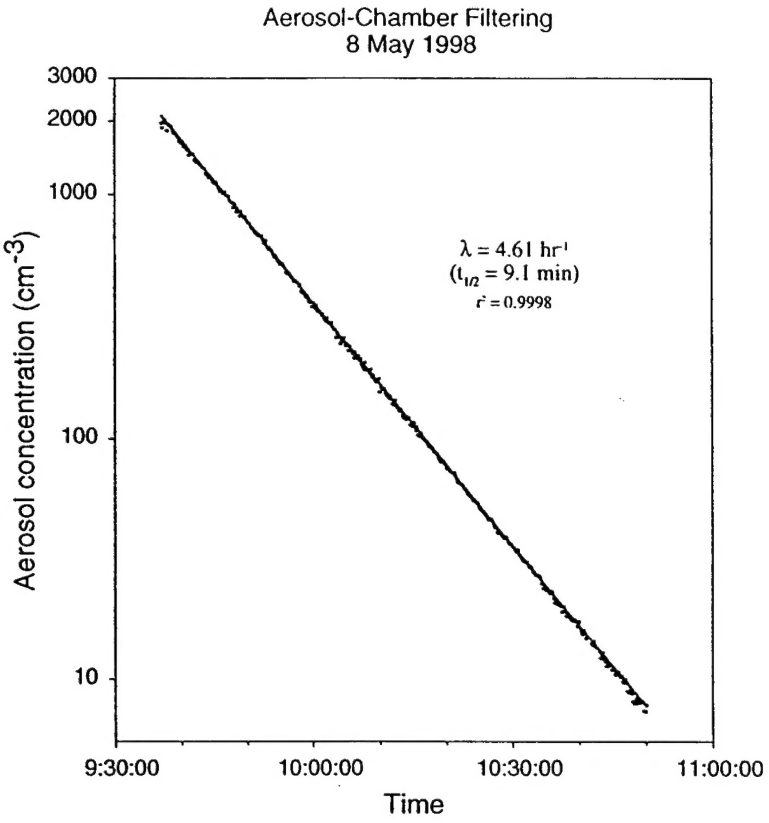

Fig. 1 – Filtering efficiency for total aerosol concentration

There are a total of 8 lamp banks containing three enclosures each for a total of 24 enclosures. All enclosures are covered with borosilicate glass (PyrexTM) windows. Each enclosure measures 17½" wide by 8½ ft tall. These lamps will be investigated separately and collectively. The data will represent the relative intensity and spectral profiles of the ultraviolet wavelength region of these various lamps.

Relative Spectral Intensity Measurements

An optical multi-channel analyzer (OMA) was used to determine the relative spectral intensity of the chamber lamp system. This instrument consists of a spectrometer with a 25 μm entrance slit and a 1200 groove per mm grating blazed at 300 nm. The measured radiation is focused onto a photo sensitive micro-channel plate. The optical signal is then stored in a computer for additional processing. Exposure times were set to 16 milliseconds in order to average out the AC effects of the lamps. The instrument's field of view was approximately 17" by 24" when located 12 ft from the desired source. The relative spectral intensity of the instrument was determined with a deuterium lamp standard.

The measured transmission of the borosilicate window is displayed in Fig. 2. A deuterium lamp standard was used as the light source for this measurement and also to correct for the spectral response of the instrument. The UV transmission begins to fall off at 320 nm and decreases to 10% of the maximum by 300 nm.

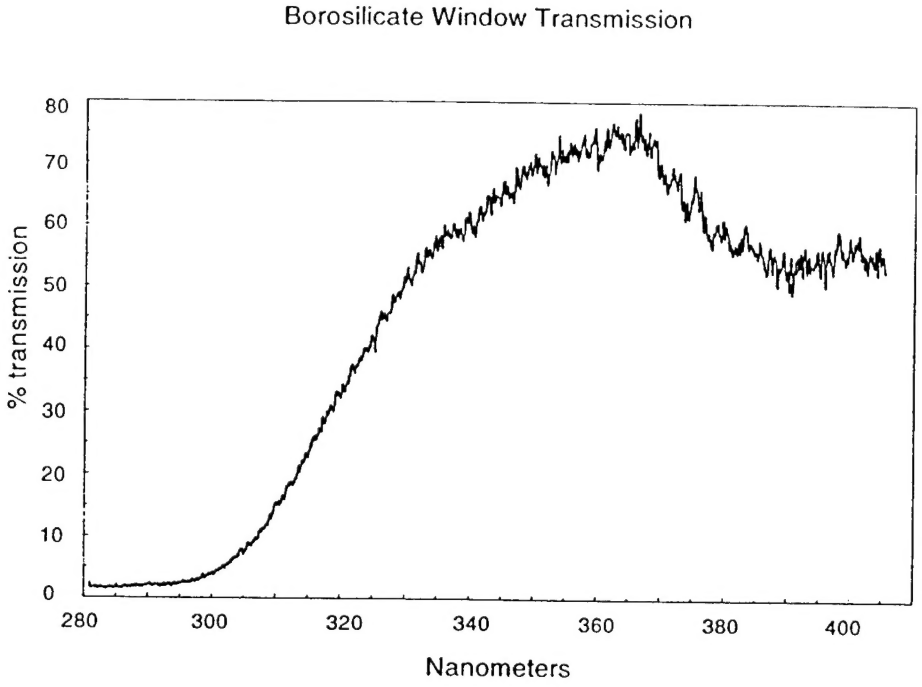

Fig. 2 – Window spectral transmission

Fig. 3 depicts the relative intensity of a single lamp enclosure with all chamber lamps operating. The instrument field of view was centered on the middle 2 ft. section of an 8.5 ft. enclosure. The actual OMA field of view represents roughly 25% of the enclosure's active area.

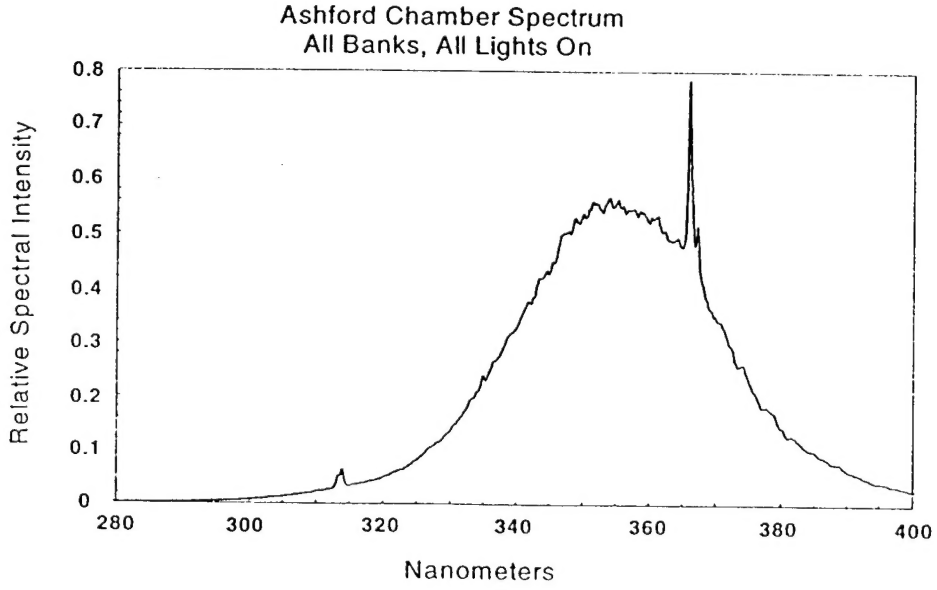

Fig. 3 – Relative intensity of a single enclosure with all lamps on

The spectrum clearly shows that the bulk of the radiation consists of the fluorescent continuum with superimposed atomic mercury lines at 365 and 312 nm. This fluorescent continuum appears centered and symmetric about the peak intensity at 355 nm. This relative spectral intensity displayed in Fig. 3 remains unchanged from that measured by Ambrusko and Wurster (1991). Although the measurement techniques differ in instrument resolution, the radiation envelope is reproduced.

Fig. 4 shows the spectral profile of the HO lamps. Fig. 5 is the spectral profile of the VHO lamps. The spectral shapes appear to be very similar.

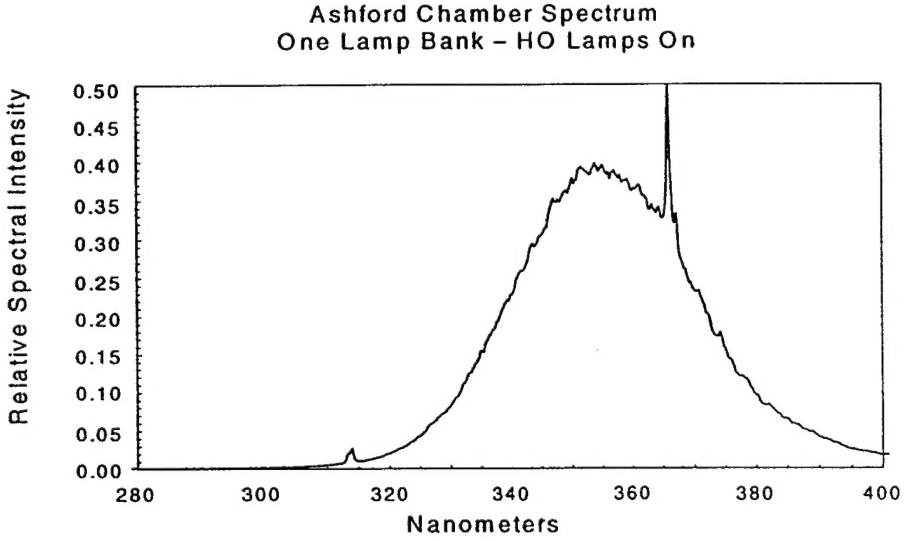

Fig. 4 – Spectral profile of the HO lamps

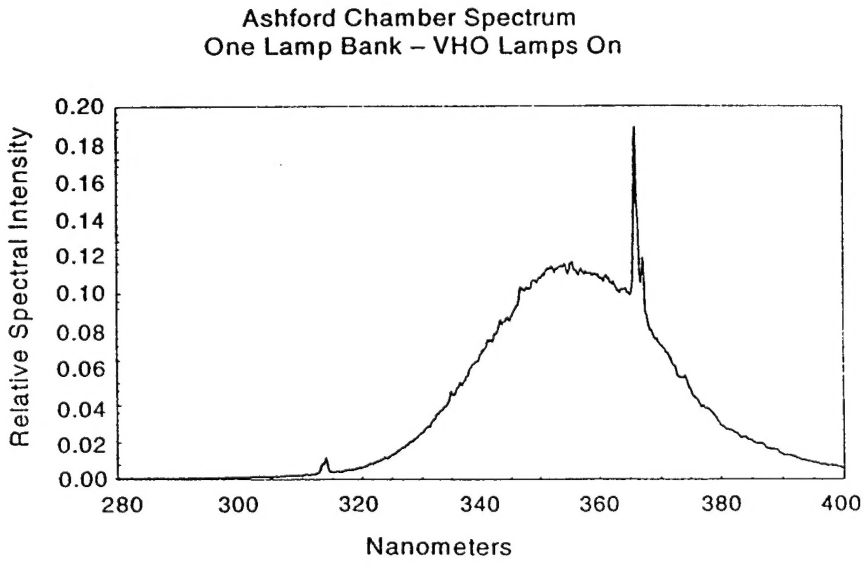

Fig. 5 – Spectral profile of the VHO lamps

Fig. 6 is the spectral profile of the FS40 lamps. The radiation peak is centered at 320 nm, dropping off more rapidly at shorter wavelengths due to the window transmission limitations. Although this spectral intensity is not large, it is the major source of short wavelength UV radiation.

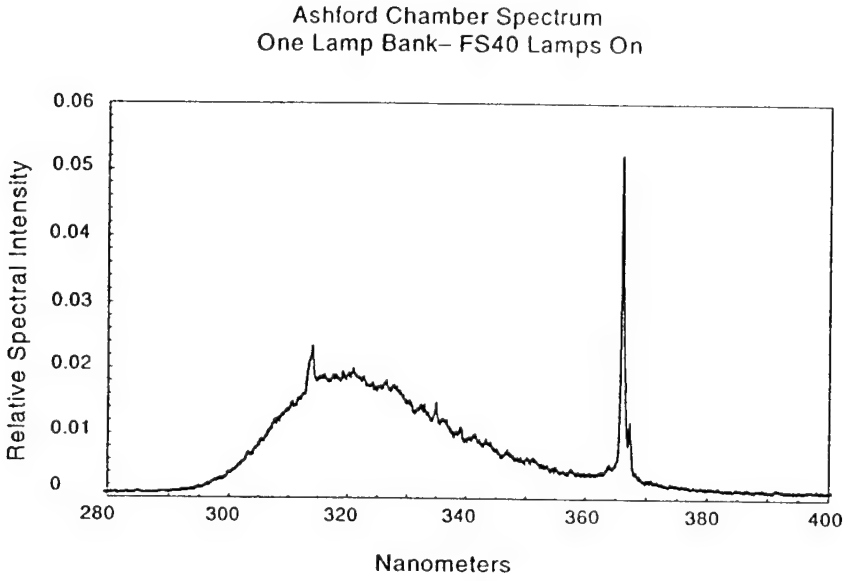

Fig. 6 – Spectral profile of the FS40 lamps

Fig. 7 is a spectral distribution with the OMA field of view shifted to a section of the chamber wall. All lamps were operating for this measurement. By comparison with Fig. 3, it can be seen that the chamber walls are spectrally neutral; they do not alter the spectrum of the incident radiation.

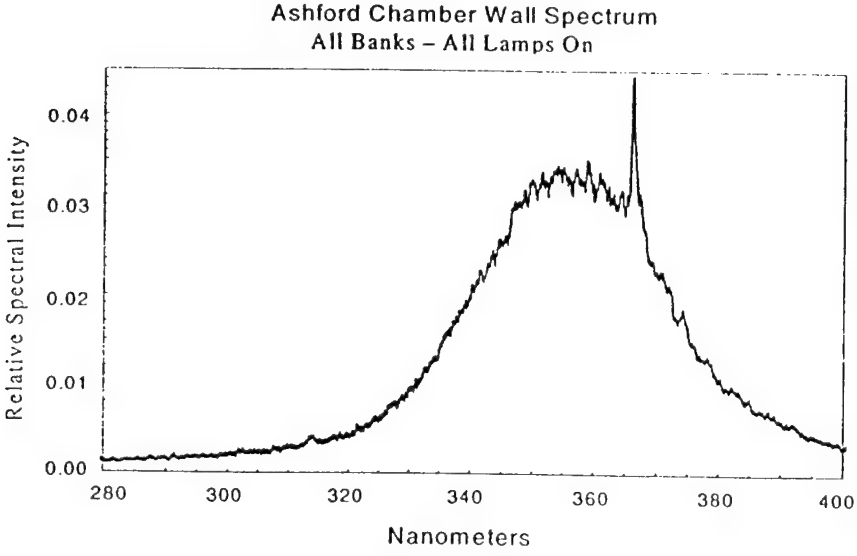

Fig. 7 – Spectral distribution with the OMA field of view shifted to a section of the chamber wall

Fig. 8 depicts an overlay of all spectra for a comparison of relative spectral irradiance. From this plot it can be seen that the HO and VHO lamps are the major radiation sources. While the FS40 lamp intensity is small, it is the dominant contributor at the shorter UV wavelengths.

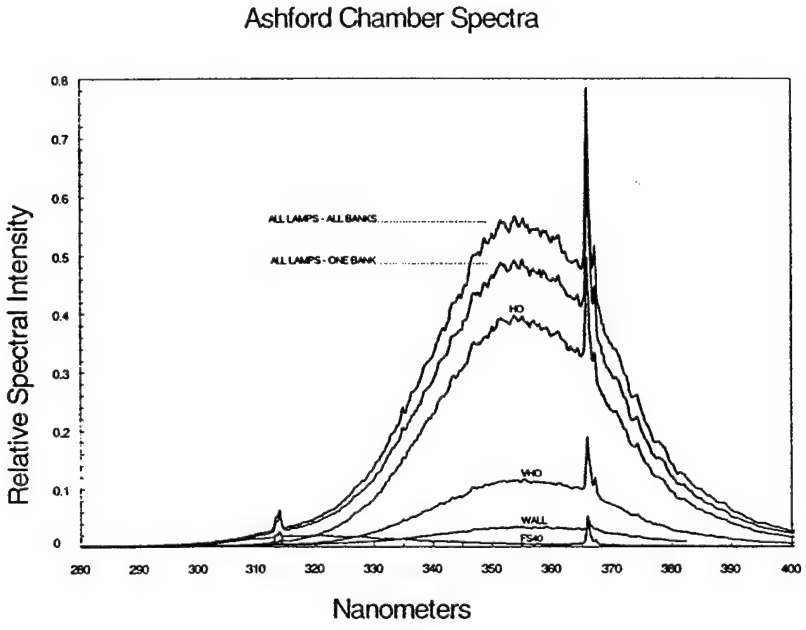

Fig. 8 – Overlay of all spectra for a comparison of relative spectral irradiance

Spectra of the lamps were also taken without the borosilicate windows in place. The relative spectral profiles of the HO and VHO lamps were not much different than the spectra taken with the windows in place. However, the FS40 lamp showed substantially more radiation below 300 nm (Fig. 9).

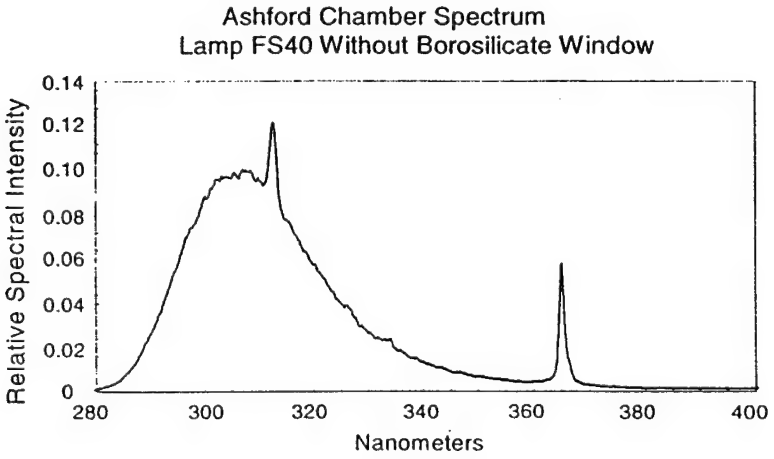

Fig. 9 – Spectra of the FS40 lamp without the borosilicate windows

UV Intensity by the Photolysis of NO_2

The chamber light intensity is also measured by the photodissociation of NO_2 in air, following the method of Stedman and Niki (1973). The procedure for this test is as follows:

1. Wash down chamber with mild detergent.
2. Rinse chamber with deionized water.
3. Fresh air flush chamber, charcoal (absolute) filter overnight with dehumidification.
4. Preheat lamps by operating for 30 minutes.
5. Turn off lamps.
6. Inject a known concentration of NO_2 into the chamber, ~1ppm.
7. Turn chamber lamps on and monitor rate of formation of O_3.
8. Turn chamber lamps off. Wait for $NO + O_3 \rightarrow NO_2 + O_2$ reverse reaction to complete.
9. Repeat steps 8 through 9.
10. Calculate k_1

$$k_1 = \frac{1}{[NO_2]_0}\frac{d[O_3]}{dt}$$

12. Calculate k_d.

$$k_d = 1.56k_1$$

An average value of k_d is determined from successive measurements. The measurements and determination of k_d are on going at this time and will be reported at a later date.

IR Transmissometer - Liquid Water Content Measurements

Measurements of liquid water content (LWC) during the phase I experiments were made using the Calspan-developed IR Transmissometer System.

Instrument Description

Path length	= 18.3 meters (folded path)
Source	= 1000 °C blackbody
Detector	= HgCdTe
Optical filter	= 11 micron narrow band pass filter, CWL = 10.939 μm, HBW = 0.655 μm

The chamber windows are made of Kodak Irtran (zinc sulfide), with 75% transmittance, 1.25 and 3 in. diameter. The mirrors consist of two 6" diameter gold coated collimating spherical mirrors and four flat gold coated turning mirrors.

Calculation of Liquid Water Content

The relation between liquid water content and IR extinction coefficient is developed in a paper by Chylek (1978). This relationship is:

$W = \beta/C$

W =Liquid water content (g/m^3)

β = Extinction coefficient (km^{-1})
C = Constant (=128 for 11 μm extinction)

This linear relationship holds for IR extinction at 11 μm wavelength and for fog drop size distribution with maximum drop radii of 14 μm.

From Beer's Law,

$$\beta = \frac{\ln(I_0 / I)}{0.0183}$$

0.0183 = Path length of IR transmissometer in km.

Substituting

$$W = \frac{\ln(I_0 / I)}{2.34}$$

where I_o is the clear chamber IR signal and I is the IR signal in fog.

Example of Data

Fig. 10 shows a plot of LWC vs. time for Cloud #1 on May 8, 1998. LWC increases to a peak value of 0.25 g/m^3 during the expansion cycle followed by a rapid decrease as the chamber is equilibrated to atmospheric pressure. The expansion for this particular case is shown in Fig. 23.

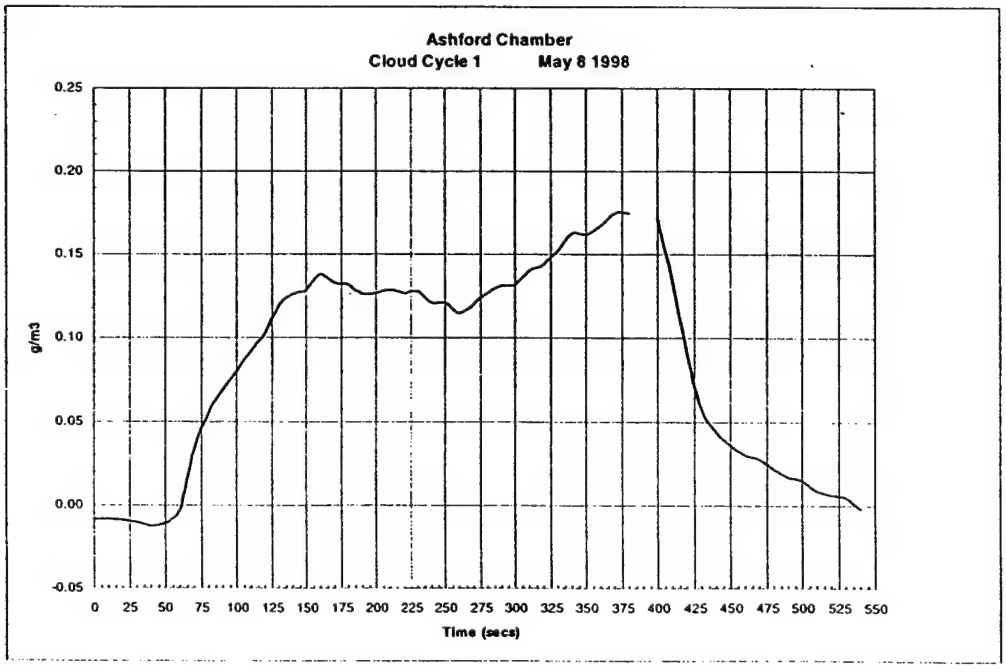

Fig. 10 – Cloud liquid water as determined by IR Transmissometer

Ozone Generator

A Welsbach Laboratory Ozonator was used to generate ozone that was introduced into the chamber when required. The instrument forms ozone by passing pure oxygen over a high voltage electrode. It can produce up to 8 grams of ozone per hour at no less than 2% weight concentration in pure, clean, dry oxygen.

The ozone is monitored by a Bendix Model 8002 ozone analyzer. The instrument utilizes the principle of photometric detection of the chemiluminescence resulting from the flameless phase reaction of ethylene gas with ozone. This instrument can detect concentrations down to 1 ppb and operates in a wide range of chamber conditions (RH=10% to 95%).

Summary and Recommendations

1. Calspan is confident they can decrease the leakage out of the chamber when it is under pressure. Recommendations concerning leaks and enlargement of the expansion valve are included in Section V on cloud processing.

2. The chamber irradiation system and spectral output of the lamps is discussed in some detail above, and the effect of this system upon photolysis of ozone is discussed later in several parts of this report. Even though the spectral response in the UV is similar to that of the solar spectrum at ground level, it may not be adequate to photolyze O_3 in the spectral region to give OH concentrations sufficient for some of the proposed experiments. The reaction may not be fast enough to measure accurately in the time frame of an experiment or to see above wall loss.

3. Calspan has some spare FS40 lamps described above and these can be mounted temporarily in the chamber for the photolysis experiments. These would not be behind the windows and therefore would have the spectral characteristics shown in Fig. 9. Therefore they should produce $O(^1D)$ and hence OH. Also available are the two portable lamp assemblies that have output only at 254 nm. As discussed later, these two lamps placed on the floor and directed upward, increased the SO_2 and particle formation when used with O_3 and dimethyl sulfide (DMS) in the chamber.

II. CHARACTERIZATION OF THE CLEAN CHAMBER

Characterization of the Chamber Contaminants

Contaminants were measured after overnight filtering through the charcoal filters and the absolute aerosol filters. SO_2, aerosols, and background hydrocarbons were measured.

There were no measurable concentrations of SO_2 (mdc 0.1 to 0.2 ppb), NO_x (mdc 1ppb), O_3 (mdc 2 ppb), and no measurable increase during 2 hours of monitoring after sealing the chamber, where "mdc" is the minimum detectable concentration.

The aerosol concentration was below 0.1 particles cm^{-3} (which we here consider to be zero) when filtering ceased and the chamber was sealed. There was typically a slow increase during chamber monitoring to values of about 10 particle cm^{-3} in two hours. The size distribution of these particles was not characteristic of newly nucleated particles (i.e. they were not ultra-fine particles.) The concentration of these particles could be attributed to make-up air leaking into the chamber to replace the air removed by the monitoring instruments. Later in the experiments when we replaced the air removed by passing an equal amount of air back into the chamber through an absolute aerosol and charcoal filters, this number was significantly reduced to the order of a few particles cm^{-3} in two hours of monitoring.

The Calspan measurements of the background hydrocarbons (HCs) in the clean chamber are continuing and the current results are being reviewed. As a back up, NRL took samples of background levels of hydrocarbons in the clean chamber on 3 days, after overnight filtering through charcoal filters and absolute aerosol filters. These samples were analyzed by the program at NRL that monitors the air in submarines. They also contributed to the interpretations given below. Both whole air and carbotrap samples were collected at the chamber and returned to NRL for analysis by gas chromatography - mass spectrometry (GCMS). The whole air samples were collected by attaching an evacuated 1 liter bulb to the chamber and allowing it to fill with chamber air. The carbotrap samples were obtained by flowing approximately 1 liter of chamber air through a carbotrap tube. Both blank tubes and a tube containing standard amounts of a variety of aromatic, aliphatic, and chlorinated hydrocarbons exposed to the same field conditions were measured for comparison.

The results from the whole air samples are shown in Table 1. In addition, the total alkanes were measured at 128 ng/l and 95 ng/l, respectively, on 5/16/98 and 5/19/98. Total aromatics were measured at 48 ng/l and 15 ng/l, respectively on 5/16/98 and 5/19/98. The sample on 5/19/98 was taken during filtering (before sealing the chamber), which may account for it being slightly cleaner.

Table 1 – Background Hydrocarbons from the Whole Air Samples

Compound Name	Sample from 5/16/98 (ppb)	Sample from 5/19/98 (ppb)
Trichlorofluoromethane	3	4
Methylene chloride	1	1
Benzene	4	2
Toluene	1	1

The results from the carbotrap samples are shown in Table 2. The chlorinated hydrocarbons are identified primarily as trichlorofluoromethane, methylene chloride, and chloroform, with some samples also containing chlorobenzene, and 1,1,2,2-tetrachloroethane. These may originate from paint outgassing or from cleaning solvents. The toluene, xylenes, and benzenes may have arisen from an uncapped pipe into the chamber that had previously been exposed to diesel exhaust and was coated with soot on the inside of the pipe. This pipe was sealed by a valve at the wall of the chamber but a portion extended into the chamber. In addition, total alkanes were measured at an average of 12 ng/l above the field blank and total aromatics were measured at an average of 59 ng/l above the field blank. These could originate from the diesel exhaust residue.

Table 2 – Background Hydrocarbons from the Carbotrap Samples

Compound Name	5/16/98 Tube #2 (ppb)	5/19/98 Tube #3 (ppb)	5/19/98 Tube #4 (ppb)	5/20/98 Tube #5 (ppb)	5/20/98 Tube #6 (ppb)
Chlorinated hydrocarbons	3	7	1	3	3
Toluene	1	2	1	1	1
Ethylbenzene	1	1	0	0	0
Xylenes	3	3	2	1	2
Trimethylbenzenes	9	17	13	7	12

Aerosol Production during the Photolysis of the Clean Chamber

Measurements were made of particle formation in a clean chamber when the chamber's irradiation lamps were turned on. Heat from these lamps raised the temperature in the chamber from 22.0 °C at 10:30 to 26.7 °C two hours later when the lamps were turned off. When the lights were turned on the particle concentration was about 20 cm^{-3}. The slow production of particles after the lights were turned on at 10:30 is shown in Fig. 11. It took about 15 minutes after the lights were turned on before a definite increase in CN was detected with the TSI 3022 CNC, and the particles did not appear in the DMA size distribution (min. radius of 0.005 μm) for about 50 minutes. The total aerosol mass produced in two hours was less than 0.1 μg m^{-3}. The source of these particles are unknown but may be related to heating of the glass windows covering the lamps. We also point out that on this first day the TSI 3025 Ultra-fine CNC was operating on the low flow settings so that diffusion losses of ultra-fine particles caused it to read approximately the same as the TSI 3022 CNC. Had it been on the higher flow range, particles would, no doubt, have appeared earlier as shown in Fig. 12. Ozone, SO_2 and NO_x concentrations all remained below the minimum detectable concentrations.

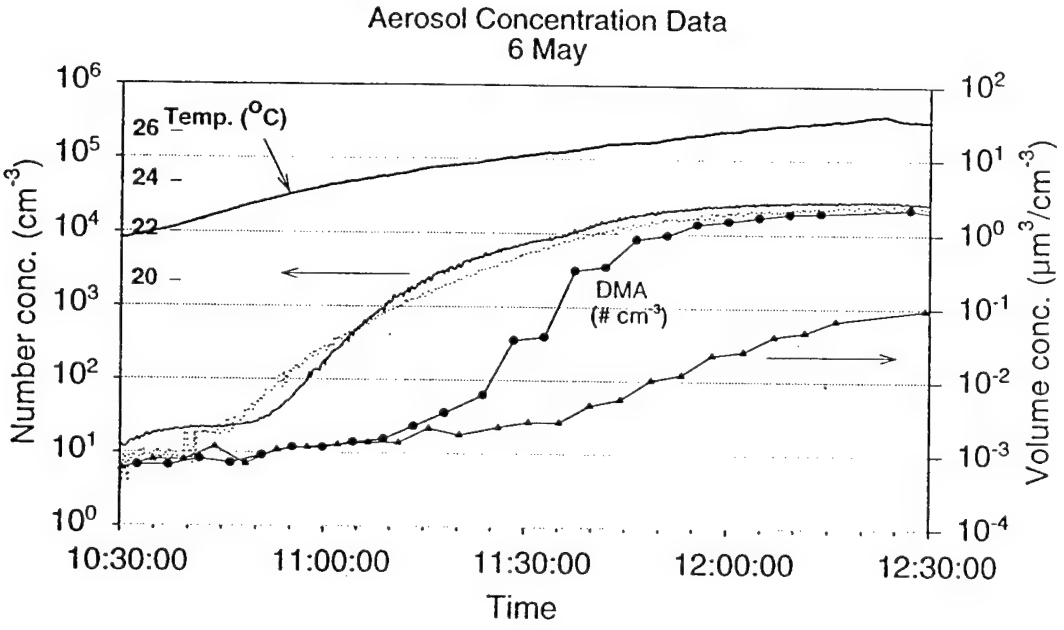

Fig. 11 – Particle formation and temperature rise during photolysis of clean chamber

A similar experiment was run on 16 May using the much weaker but shorter wavelength (0.254 μm) lamps that NRL had brought, which are described later. These cooler lamps produced no particles in a clean chamber and no noticeable temperature increase.

Aerosol Production with O_3 as the Only Reactant in the Clean Chamber

Fig. 12 shows particle production when O_3 was introduced into a clean chamber at 10:35 on 16 May. Ultra fine particles appear within 5 minutes. These particles grew into the range detected by the TSI 3022 CNC in about 10 minutes, but even after an hour all particles were smaller than 0.005 μm, the

minimum size detectable by the DMA. The mass (volume) is calculated from the NRL DMA that scanned a size distribution about every 4.5 minutes. Values of mass below about 0.001 μg m^{-3} are in the noise level of the measurement. The source of these particles in a "clean" chamber is thought to be the result of the production of reaction products of ozone with residual non-methane hydrocarbons (NMHC) in the chamber.

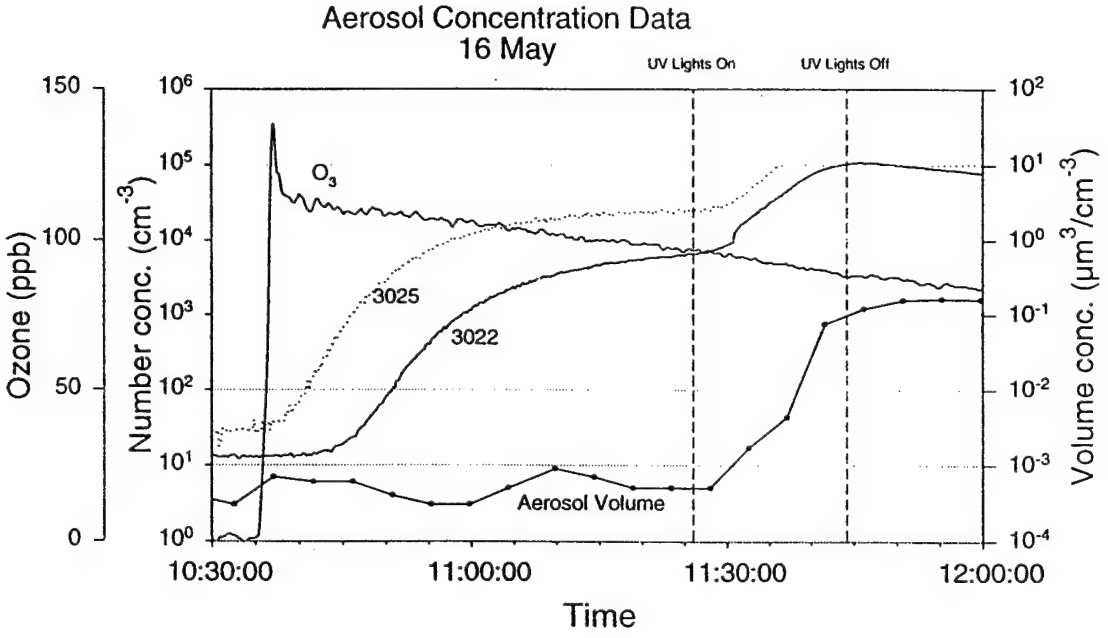

Fig. 12 – Aerosol production in clean chamber with Ozone present

If the chamber's irradiation system is turned on after particle formation caused by the earlier introduction of O_3, no additional particles are formed. However if the short wavelength (254 nm) portable lamps supplied by NRL are placed in the chamber, then we see additional particle and mass formation as shown after 11:30 in Fig. 12. We interpret these results to indicate that the existing chamber irradiation lamps do not produce sufficient short wave radiation to produce $O(^1D)$ and hence OH during photolysis of O_3 to produce observable OH oxidation in the chamber. On the other hand, the much weaker UV lamps effectively photolyze ozone to OH causing some unknown reaction to occur. This unknown reaction may be oxidation of background NMHC in the chamber. The mass of aerosol produced in the clean chamber photolysis of O_3 by the UV lamps is clearly observable after 11:30 as shown in Fig. 12, but it is very small, reaching only about 0.15 μg m^{-3}.

Aerosol Production with SO_2 as the Only Reactant in the Clean Chamber

No particle formation was observed when SO_2 was the only reactant injected into a clean chamber. (7 May, 10:40-11:39)

Summary and Recommendations

1. We recommend that CUBRC provide a system to supply make-up air to the chamber at a rate removed by the investigators. This air should be introduced through absolute aerosol filters and charcoal filters. While the amount of air removed is very small compared to the volume of the chamber, seepage in of make up air from the building of only 0.01% will increase the aerosol concentration from zero to 10 particles cm^{-3} if the concentration in the building is 10K particles cm^{-3}. This is approximately what we saw over a two hour period when only the NRL sampling was running. This should be a variable air flow, which can be adjusted as investigators tell the operator how much air they are removing.

2. Characterizing the background HCs in the chamber, finding their source, and making an effort to reduce them should continue. We laud Calspan's continuing effort in making measurements with and without the mixing fan on to see if the fan motor is causing any build up of HCs after sealing of the chamber.

3. We need an estimate of the SO_2 and DMS oxidation when ozone is added to the chamber. We assumed that ozone did not react with either SO_2 or DMS, but now have been informed that there is some reaction of SO_2 with ozone. We attributed all particle formation when ozone and SO_2 were added to the chamber as a result of ozonides (Criegee intermediates) formed by reaction of ozone with background HCs, which subsequently reacted with SO_2 to form sulfuric acid. Is it possible to explain our result by direct reaction of SO_2 and ozone?

III. WALL LOSS OF REACTANTS AND AEROSOLS AND PHOTOLYSIS LOSS OF O_3

Determinations of wall losses in a clean chamber were made for O_3, SO_2, cyclohexene, alpha-pinene, DMS and aerosols. The hydrocarbon losses were determined from five GCFI (gas chromatograph - flame ionization detector) samples taken every half hour over a two hour period. Cyclopentene was not analyzed because interference from the GC solvent rendered the GC data unusable for cyclopentene. All wall loss determinations given here were made with the mixing fan on.

Under the well-mixed approximation (concentrations in the chamber are uniform throughout the chamber except in a shallow layer [diffusion sublayer] close to the wall), the decay resulting from wall loss can be written as an exponential decay process:

$$\frac{n(t)}{n(0)} = \exp(-\lambda t) = \exp\left(-\frac{S}{V} v_d t\right)$$

where λ the decay constant, S/V is the ratio of the chamber surface area to volume which for the Calspan chamber is 0.67 m^{-1}, and v_d is the deposition velocity. λ is just the fractional loss per unit time:

$$\frac{1}{n}\frac{dn}{dt} = -\lambda$$

The wall losses described below were obtained by fitting the experimental data to the above expression and are given both in terms of the decay constant and the deposition velocity.

minimum size detectable by the DMA. The mass (volume) is calculated from the NRL DMA that scanned a size distribution about every 4.5 minutes. Values of mass below about 0.001 μg m^{-3} are in the noise level of the measurement. The source of these particles in a "clean" chamber is thought to be the result of the production of reaction products of ozone with residual non-methane hydrocarbons (NMHC) in the chamber.

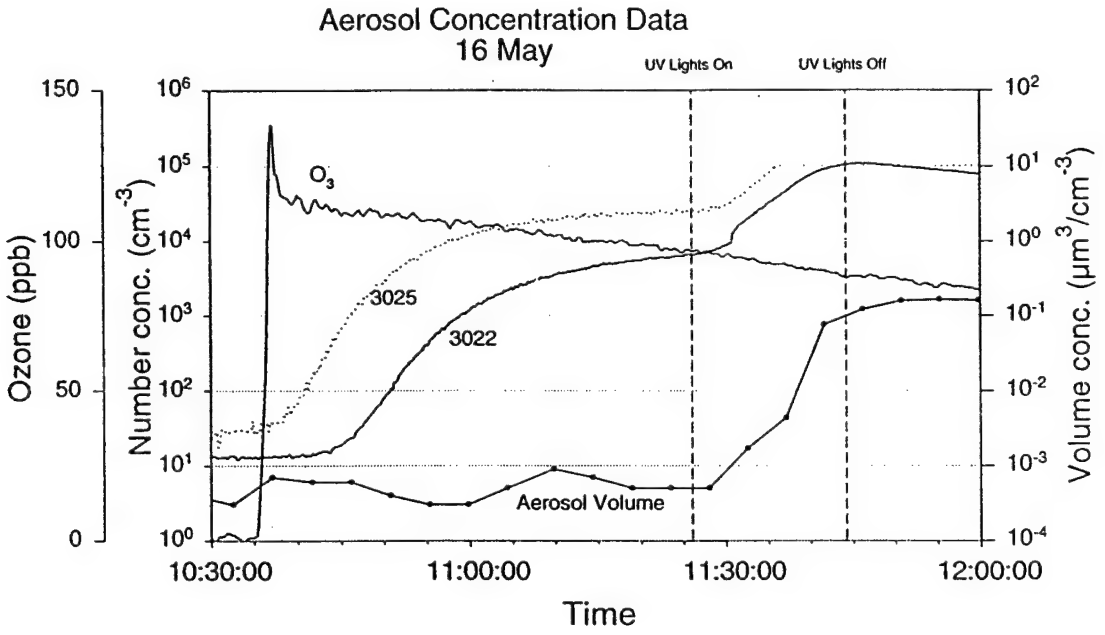

Fig. 12 – Aerosol production in clean chamber with Ozone present

If the chamber's irradiation system is turned on after particle formation caused by the earlier introduction of O_3, no additional particles are formed. However if the short wavelength (254 nm) portable lamps supplied by NRL are placed in the chamber, then we see additional particle and mass formation as shown after 11:30 in Fig. 12. We interpret these results to indicate that the existing chamber irradiation lamps do not produce sufficient short wave radiation to produce $O(^1D)$ and hence OH during photolysis of O_3 to produce observable OH oxidation in the chamber. On the other hand, the much weaker UV lamps effectively photolyze ozone to OH causing some unknown reaction to occur. This unknown reaction may be oxidation of background NMHC in the chamber. The mass of aerosol produced in the clean chamber photolysis of O_3 by the UV lamps is clearly observable after 11:30 as shown in Fig. 12, but it is very small, reaching only about 0.15 μg m^{-3}.

Aerosol Production with SO_2 as the Only Reactant in the Clean Chamber

No particle formation was observed when SO_2 was the only reactant injected into a clean chamber. (7 May, 10:40-11:39)

Summary and Recommendations

1. We recommend that CUBRC provide a system to supply make-up air to the chamber at a rate removed by the investigators. This air should be introduced through absolute aerosol filters and charcoal filters. While the amount of air removed is very small compared to the volume of the chamber, seepage in of make up air from the building of only 0.01% will increase the aerosol concentration from zero to 10 particles cm^{-3} if the concentration in the building is 10K particles cm^{-3}. This is approximately what we saw over a two hour period when only the NRL sampling was running. This should be a variable air flow, which can be adjusted as investigators tell the operator how much air they are removing.

2. Characterizing the background HCs in the chamber, finding their source, and making an effort to reduce them should continue. We laud Calspan's continuing effort in making measurements with and without the mixing fan on to see if the fan motor is causing any build up of HCs after sealing of the chamber.

3. We need an estimate of the SO_2 and DMS oxidation when ozone is added to the chamber. We assumed that ozone did not react with either SO_2 or DMS, but now have been informed that there is some reaction of SO_2 with ozone. We attributed all particle formation when ozone and SO_2 were added to the chamber as a result of ozonides (Criegee intermediates) formed by reaction of ozone with background HCs, which subsequently reacted with SO_2 to form sulfuric acid. Is it possible to explain our result by direct reaction of SO_2 and ozone?

III. WALL LOSS OF REACTANTS AND AEROSOLS AND PHOTOLYSIS LOSS OF O_3

Determinations of wall losses in a clean chamber were made for O_3, SO_2, cyclohexene, alpha-pinene, DMS and aerosols. The hydrocarbon losses were determined from five GCFI (gas chromatograph - flame ionization detector) samples taken every half hour over a two hour period. Cyclopentene was not analyzed because interference from the GC solvent rendered the GC data unusable for cyclopentene. All wall loss determinations given here were made with the mixing fan on.

Under the well-mixed approximation (concentrations in the chamber are uniform throughout the chamber except in a shallow layer [diffusion sublayer] close to the wall), the decay resulting from wall loss can be written as an exponential decay process:

$$\frac{n(t)}{n(0)} = \exp(-\lambda t) = \exp\left(-\frac{S}{V} v_d t\right)$$

where λ the decay constant, S/V is the ratio of the chamber surface area to volume which for the Calspan chamber is 0.67 m^{-1}, and v_d is the deposition velocity. λ is just the fractional loss per unit time:

$$\frac{1}{n}\frac{dn}{dt} = -\lambda$$

The wall losses described below were obtained by fitting the experimental data to the above expression and are given both in terms of the decay constant and the deposition velocity.

Ozone Wall Loss and Ozone Photolysis Rate

Fig. 13 shows the O_3 wall loss to be about 16% per hour when O_3 was the only reactant in the chamber. The O_3 loss was increased when the chamber's irradiation lights were turned on. We attribute the additional loss of O_3 to be the result of photolysis of O_3. If we assume the two losses to be additive, we obtain a decay constant for photolysis of about 11% per hour. The same type of measurement was made on 20 May, except that the portable NRL UV lights were used. These lights, as discussed later, have much less total irradiation intensity, but the wavelength is at 0.254 μm and gives rise to more $O(^1D)$ (and therefore more OH). The photolysis rate of O_3 measured with these lights is only about 4% per hour. Even though the photolysis rate for the UV lamps are less than for the chamber lamps, the wavelength is in a region of the spectrum that produces $O(^1D)$, and hence we expect OH formation to be greater. This was found to be the case as discussed in Section II and will be evident from additional data given later. Ozone losses were also calculated independently using data from the Calspan ozone monitor. Values for several different measurement periods are given in Table 3 at the end of Section III.

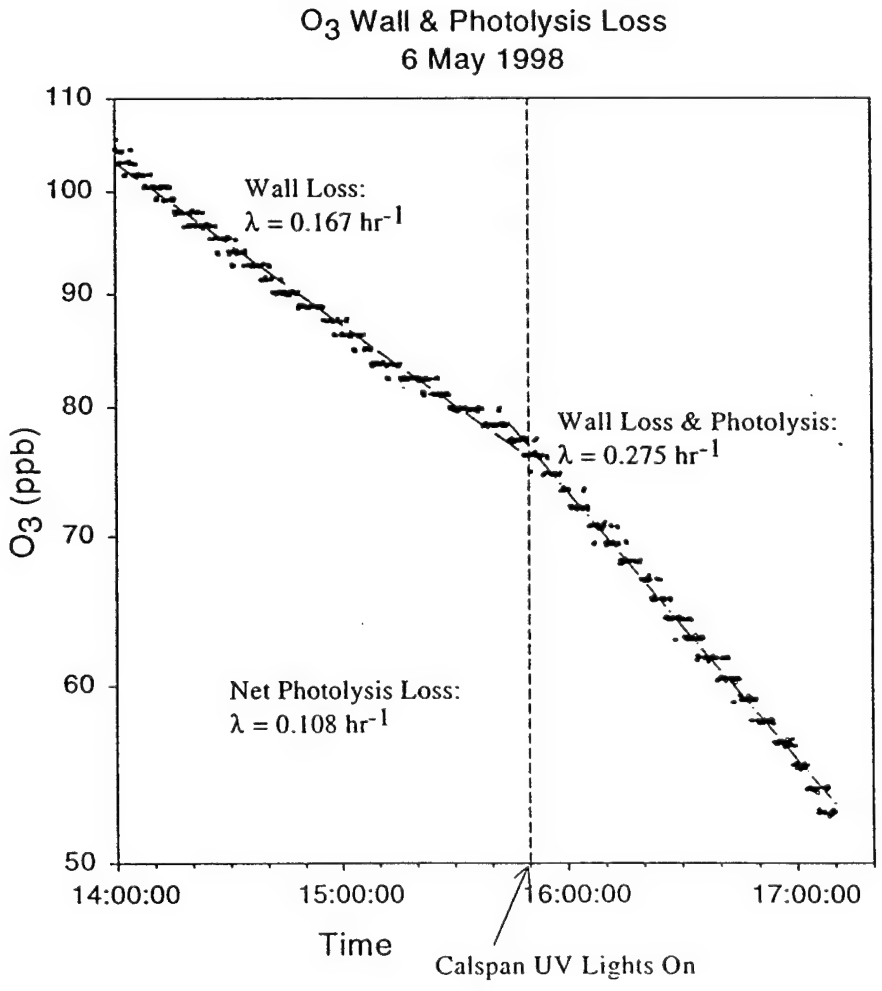

Fig. 13 – O_3 wall and photolysis loss

SO_2 Wall Loss

Wall losses for SO_2 are more severe than for O_3, as would be expected, and are illustrated in Fig. 14 when SO_2 was the only reactant in the chamber. Wall losses of SO_2 approached 90% per hour and were more variable from day to day than O_3. Also shown in Table 3 (at the end of this section) are values for two cases when SO_2 and O_3 were both injected into a clean chamber. The lower values (about 76%) are not believed to be the result of the presence of O_3, but merely the result of day-to-day variations. Additional illustrations of SO_2 wall losses and the variably can be seen in Figs. 39 and 40, during measurements of SO_2 uptake by sea-salt aerosol. The wall loss during these heterogeneous experiments ranged from about 75% to 100% per hour. These higher values may be a result of salt on the walls caused by the high salt loading during these latter experiments. To increase the accuracy of the heterogeneous chemistry measurements, wall losses were measured before and after each sea-salt aerosol injection as will be discussed in section VIII.

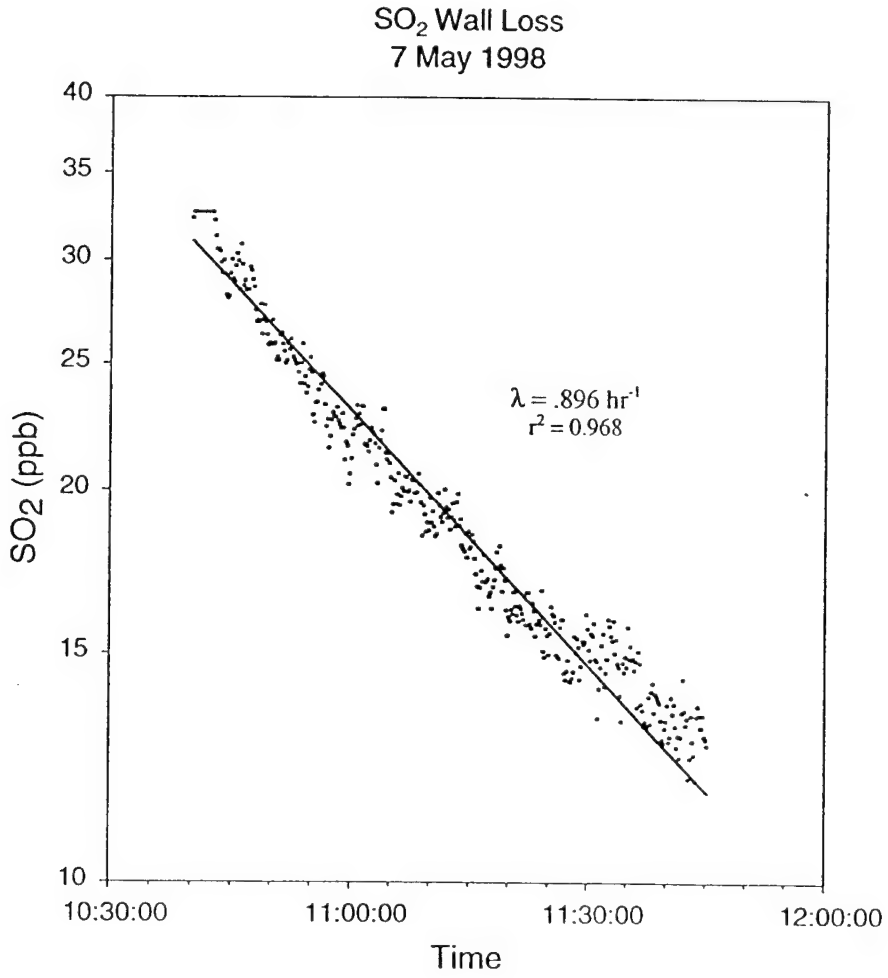

Fig. 14 – SO_2 wall loss in clean chamber

Hydrocarbon Wall Loss

Wall loss measurements of cyclohexene, α-pinene and DMS were made by injecting each HC into a clean chamber and observing the concentration every half hour during a two hour period. The GC methodology and calibration for all GC measurements are given in Appendix A. Figs. 15 through 17 show the results for the wall loss measurements. The calculated concentrations introduced into the chamber were 50 ppb, 10 ppb and 30 ppb for cyclohexene, α-pinene and DMS, respectively.

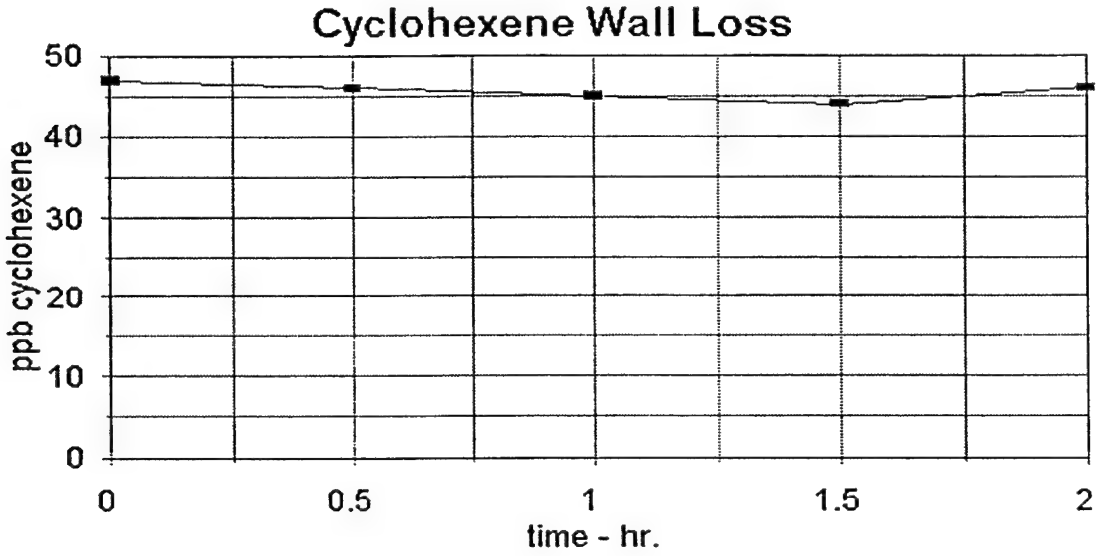

Fig 15 – Wall loss for cyclohexene

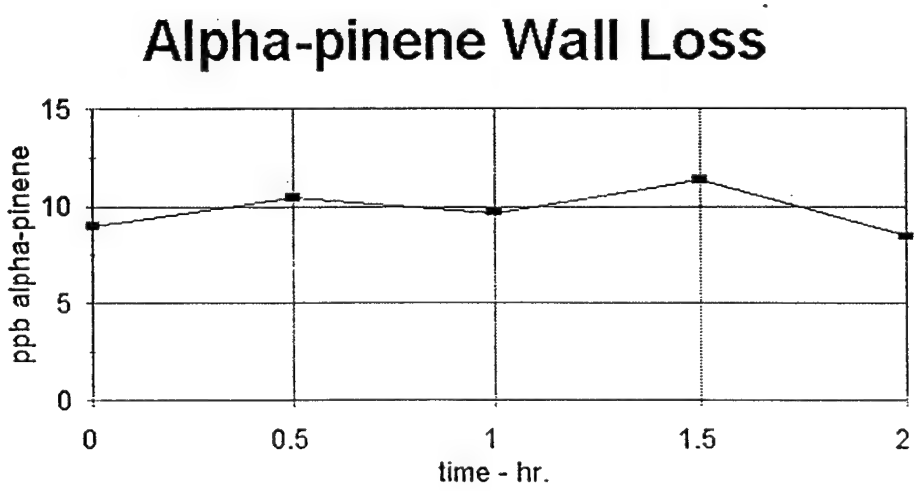

Fig. 16 – Wall loss for alpha-pinene

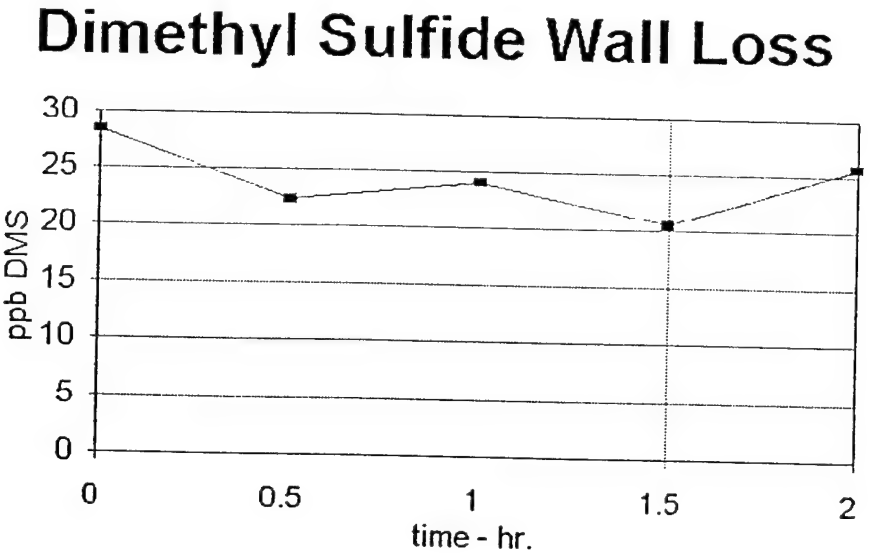

Fig. 17 – Wall loss for DMS

Within the accuracy of the measurements no wall loss was observed for any of the three HCs over the two hour period.

Aerosol Wall Loss

Aerosol losses are due to coagulation and wall losses. For monodisperse particles the coagulative loss goes as the square of the concentration, whereas the wall loss goes as the first power of the concentration. For monodisperse aerosols the characteristic time for coagulative loss is about 5 hours for concentrations of 100,000 cm^{-3}, and 50 hours for concentrations of 10,000 $\cdot cm^{-3}$. Wall losses were calculated for three periods of time when the size distribution was strongly peaked (nearly monodisperse) and the concentrations were low enough (< 80,000 cm^{-3}) for coagulative losses to be ignored. One period is illustrated in Fig. 18, and the results of all three periods given in Table 3. The radius of the peak in the size distribution is given in each case in Table 3. The particles were smallest on 6 May and give the largest deposition velocity, which is reasonable since smaller particles have higher diffusion coefficients. The particles were least monodisperse on 7 May. A quantity of interest is the (diffusion) sublayer distance, δ, of the chamber defined by the ratio of the diffusion coefficient to the deposition velocity. For the three days listed in Table 3, the values of δ are about 32, 10 and 20 μm respectively. On the first day (6 May). which gave a value of 32 μm, the size distribution was the most monodisperse. It will be interesting to run this data using a more comprehensive numerical aerosol model to obtain a chamber δ and see if it is more constant than indicated above.

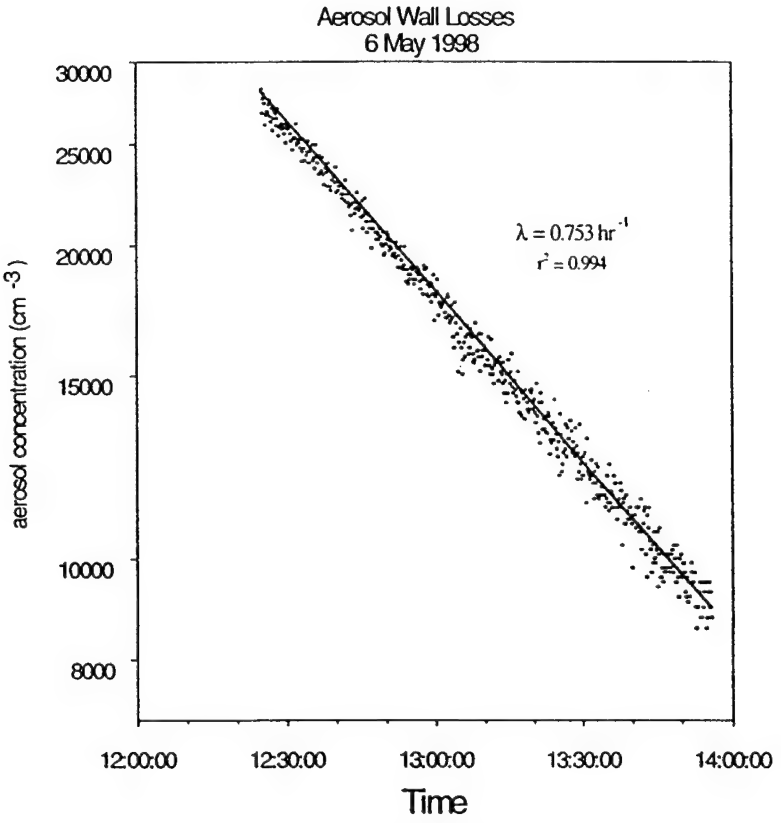

Fig. 18 – Aerosol wall loss

Table 3 – Wall Losses

	Date	Comment	λ (hr^{-1})	Correlation	v_d ($cm\ s^{-1}$)
O_3	6 May	NRL Dasibi	0.17	0.99	0.0069
	6 May	Calspan Bendix	0.15	0.996	0.0062
	16 May	Calspan Bendix	0.2	0.99	0.0083
	20 May	NRL Dasibi	0.16	0.981	0.0067
O_3 (Photolysis)	6 May	Calspan Lights, NRL	0.11		NA
	6 May	Calspan Lights, Cal.			
	20 May	NRL Lights	0.04		NA
SO_2	7 May		0.9	0.962	0.037
	7 May	with O_3	0.77	0.968	0.032
	15 May	with O_3	0.75	0.998	0.031
		Radius at peak			
Aerosol	6 May	0.011 μm	0.75	0.994	0.031
	7 May	0.027 μm	0.43	0.998	0.018
	20 May	0.022 μm	0.36	0.985	0.015

Summary and Recommendations

Wall losses of O_3 in a clean, dry chamber are about 17% hr^{-1} and fairly constant from day to day when compared to SO_2 which exhibited wall losses typically about 85% hr^{-1} with values ranging between 75% and 100% hr^{-1}. No wall losses were observed for cyclohexene, α-pinene, or DMS over a two hour period within the accuracy of the measurement (about 20%). Wall losses for particles when the size distribution peaked at a radius of 0.011 μm were about 75%, and 36% when the size distribution peaked at 0.22 μm. (These were dry sizes as measured with the DMA; i.e. did not account for the RH in the chamber.)

IV. NEBULIZER CHARACTERIZATION

Two types of size distribution produced by nebulizers will be required: (1) one with a peak in the size distribution in the 0.5 to 3.0 μm radius range for heterogeneous chemistry experiments and with capacity to nebulize solutions at the rate the order of liters per hour, and (2) the other with the ability to produce particles with a peak in the 0.02 to 0.03 μm radius range, and concentrations in the range of several hundred to several thousand for cloud processing experiments.

Description of Particles Produced with Calspan Nebulizer

The Calspan chamber is equipped with a nebulizer with a variable capacity (by changing inserts and air pressure) to nebulize solutions at rates of liters to tens of liters per hour. This nebulizer is mounted in the ceiling of the chamber and appears to be adequate to generate the sea-salt particle distribution required for the heterogeneous sea-salt experiments. The compressed air source for these experiments is research grade N_2 from a cylinder. Tests were run with solutions of real seawater (~3.5 g of salt per liter) and enriched sea water solutions generated by mixing artificial sea salt (obtained from Aldrich) in concentrations of 11 g/l and 35 g/l. The size and mass distributions for sea water are shown Figs. 19 and 20 at four times over the 15 min. period during which the nebulizer was operating. We have plotted only one of the four PMS-OPC ranges for clarity. For this data the nebulization rate was about 1.8 liter per hour with 35 PSI applied to the nebulizer. Higher solution concentrations of sea-salt can be used if more buffering is required. The mass loading (assuming unit density) is given in Fig. 20 and reached 0.015 g m^{-3} in about 15 minutes. The smaller particles continue to increase but the larger particles start to come to equilibrium by the end of 12 minutes. The high variability in the largest channels is due to counting statistics. There are very few large particles by number even though they contain a significant amount of the mass. The data shown were taken at about 85% relative humidity.

The size distributions were only marginally different using the more concentrated solutions (radius is proportional to the cube root of the mass). The test was not run for a sufficient period of time to observe saturation in the size range that was plotted ($r< 8$ μm). Had we run the test longer, we undoubtedly would have seen the concentrations of the largest particles come to steady state between production and deposition. Since the concentration of the larger particles shown in Fig. 20 had not saturated in 15 minutes we can assume that the mean lifetime of the particles (with $r<8$ μm) is greater than 10 minutes. This should be more than enough time for particles to suffer the SO_2-O_3 reaction postulated.

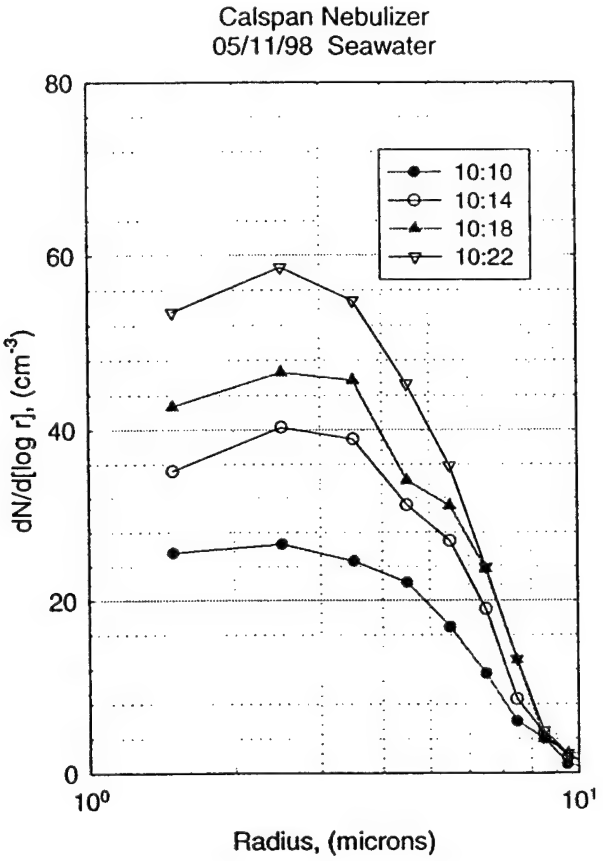

Fig. 19 – Size distribution produced by Calspan nebulizer

TSI 9302 Nebulizer

The TSI 9302 is a small nebulizer that produces solution droplets of about 0.3 microns. The solution to be nebulized must be very dilute to produce CCN with (dry) radii of 0.02 microns. Two (dry) size distributions are shown in Fig. 21; both were taken after about 15 minutes of nebulization in the chamber. The solid circles were for a solution of 102 mg of sea-salt per liter of water, and the open circles for a solution of 6.1 mg of ammonium sulfate per liter of water. The rate of particle production was about half that of sea salt solution for the lower concentration of ammonium sulfate. The total particle concentration after 15 minutes of nebulization was 1830 for the sea-salt solution whereas it was only 960 for the ammonium sulfate solution. The peak in the size distribution was at about the same radius in both cases. It is difficult to explain the observed behavior in detail since one would have expected the number concentrations of dry particles to be nearly the same and the peaks shifted according to the cube root of the solution concentration (mass), if the nebulizer produced droplets which were the same in both cases. We also made a run with triply distilled water and found a much lower production rate (only about 50 particle cm^{-3} after half an hour) with size peak in the .005 to .008 μm radius range. For distilled water some of the particles may have been below the detection limit (.005 μm) of the DMA.

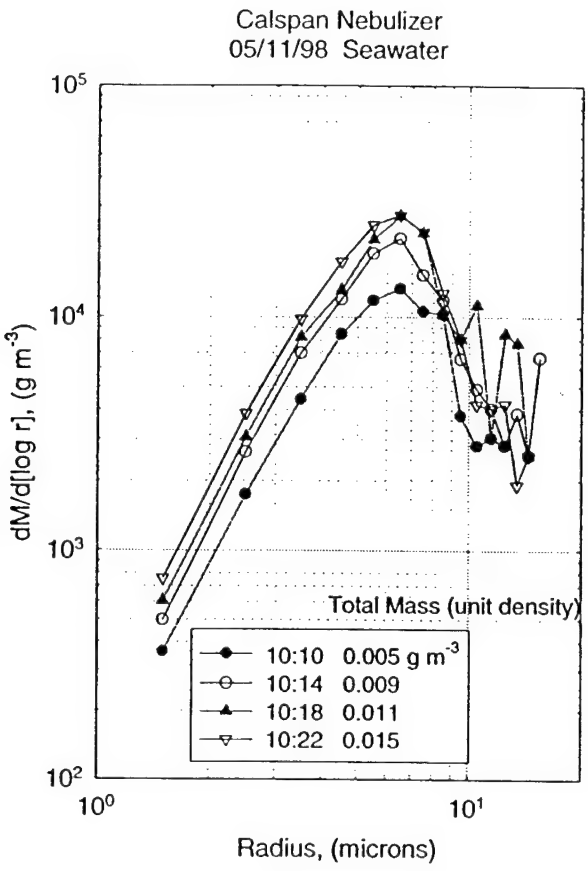

Fig. 20 – Mass distribution generated by the Calspan nebulizer

Summary and Recommendations

1. The Calspan nebulizer appears to be adequate for the heterogeneous sea-salt experiments as we now envision them. The amount of material introduced and the size and resulting residence time of the particles seem to be adequate for the postulated reaction to take place. The particles are introduced at the top of the chamber and about one and a half meters in from the wall. The upward directed mixing current in the center of the chamber causes a downward current along the wall. The spray from the downward directed nebulizer together with the downward air current have a tendency to drive the droplets rapidly downward. To counter this downward flow the fan, during the heterogeneous experiments, should be placed directly below the nebulizer, this aids in suspending the droplets and gives them more time to evaporate before encountering a downward draft.

2. The TSI 9302 also appears to be adequate for cloud processing and cloud microphysics studies. Since the concentrations of the solutions must be so dilute to generate CCN in the range desired, it may be difficult (but possible) to make accurate mixtures of particle composition as proposed in the Science Plan under "Effects of Organics on Cloud Activation".

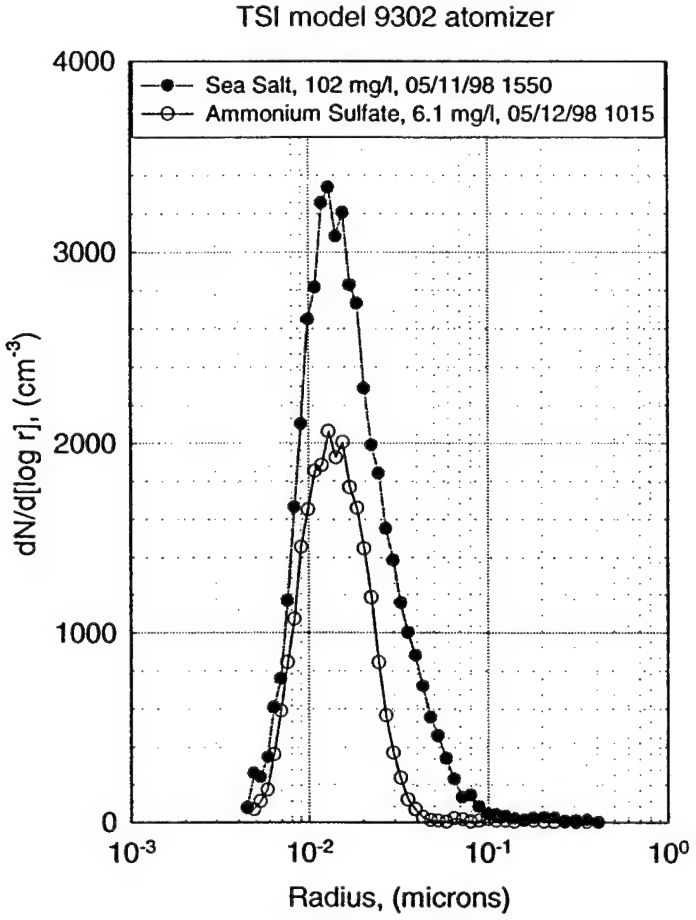

Fig. 21 – Size distribution produced by TSI 9302 nebulizer

V. CLOUD PROCESSING

Cloud processing experiments were conducted on 8, 9 12, 14, 15, and 16 May. These experiments tested not only the cloud processing procedures and chamber capabilities, but also the introduction of reactants and the ability of monitoring equipment to observe and quantify the effects of cloud processing.

Cloud Formation in the Chamber

After the desired seed nuclei are generated in the chamber, the chamber is humidified by injecting deionized water from a tube around the top of the chamber wall. A series of nozzles directs a stream of water against the wall and the water flows down the wall and puddles on the floor of the chamber. The initial increase in humidity is fairly rapid and approaches saturation exponentially. When the chamber is nearly saturated (dew point depression is less than a degree) the chamber is over-pressured to about 20 mbar for ten minutes. The compression slightly heats the chamber but the dew point depression recovers its low value within ten minutes. The air providing the overpressure is supplied through the charcoal and absolute aerosol filters, and a small amount of air must continually be supplied during the compression to

maintain the pressure against small leaks in the air handling system. During the overpressure period any required reactants can be supplied to the chamber and the mixing fan remains on until just before the start of the expansion. The expansion of the air in the chamber is accomplished by exhausting air from the chamber through a three inch diameter ball valve connected to a vacuum blower. The expansion through the blower is continued until the pressure in the chamber is about 10 mbar below ambient. Expansion by this system was not adequate for all desired expansions, so during the characterization experiments an additional two inch ball valve was installed which could be used during the initial expansion while the chamber pressure was still above ambient pressure. After the cloud is held the desired length of time (usually 3 to 4 minutes) the chamber is allowed to come back to ambient pressure by admitting air through the filters. The purpose of the compression at the end is to evaporate the cloud in a definitive manner. The saturation ratio in the chamber (at 293 °C) is given by

$$dS = -4.196\frac{dP}{P} - 1.841X10^5 dM \qquad (1)$$

where M is the liquid water (g cm^{-3}) formed during the expansion dP. The numerical constants are temperature dependent. M is calculated from the droplet activation and growth equation.

Before any liquid water (cloud) is formed the rate of increase of S is given by the first term. If the chamber is not saturated at the time the expansion begins, some of the expansion must be used to obtain saturation. For example if the dew point depression is 1.5 °C, then at 20 °C the saturation ratio is 0.91 and it would require 21 mbar of expansion to reach saturation. Once the chamber reaches saturation it requires only 0.8 mbar of further expansion to supersaturate the chamber to 0.33% (saturation ratio of 1.0033); at that point ammonium sulfate particles of 0.03 μm radius and larger would be activated.

The above calculations assume no liquid water is formed. Equation (1) can also be used to predict the liquid water formed during the expansion from the point of saturation. At the end of the expansion the cloud droplets are large enough so that their surface vapor pressure is nearly the saturation vapor pressure of pure water. Therefore $\Delta S=0$, and ΔM (total liquid water formed) is uniquely given by ΔP, which is the total pressure drop (starting at the point of saturation). For each 10 mbar of expansion, 0.22 g m^{-3} of liquid water is formed . Therefore if we start at 20 mbar over-pressure and at saturation, then expand to 10 mbar below ambient pressure, we could expect to have a cloud with a LWC of about 0.6 g m^{-3}. During the characterization experiments we were not able to get the dew point depression much smaller than 1 °C and the liquid water never did approach the maximum value just given. The reason for this, we believe, may have been that the floor of the chamber was colder than the upper part of the chamber. The vapor pressure was mainly determined by the water on the floor - the water runs quickly down and off the walls. As will be discussed later this can probably be remedied in the next phase of experiments by adding some heating to the space under the floor of the chamber while monitoring the wall temperature at several points.

We have a complete cloud microphysical model that treats the activation and growth of cloud droplets starting from activation of the aerosol (provided we know the aerosol composition). This predicts the number and size distribution of cloud droplets (liquid water) from the precursor aerosol size distribution and expansion rate in the chamber. This model is coupled with a chemical module for SO_2 oxidation by O_3 and H_2O_2 and will be briefly described later.

Growing in Sulfuric Acid Seed Nuclei from Gas-Phase Reaction Products

A cloud precursor aerosol size distribution with a very steep slope is ideal for observing the effect of cloud processing. Such a size distribution can be produced by nucleation and condensation growth of

particles from the gas-phase reaction of O_3 and SO_2. Presumably the O_3 reacts with residual NMHCs in the chamber forming an ozonide which reacts with SO_2 forming H_2SO_4 which condenses as an aerosol.

Such a procedure is shown in Fig. 22 (data from 9 May 0845-1020). However this procedure is time consuming and is expected to become even slower as ways to decrease the background NMHC in the chamber are found. The process may be speeded up by adding a small amount of pentene (ethene was found to be ineffective). Photolysis of the O_3 already in the chamber would be expected to generate OH, which in turn would increase the rate of oxidation of SO_2, increasing the aerosol growth rate. However it was found that the chamber's irradiation system (which simulates the solar spectrum at ground level) did not noticeably increase the aerosol growth rate. NRL brought two irradiation lamps that produced irradiation at 254 nm. These lamps, when placed in the chamber, did indeed substantially increase the rate of aerosol mass formation. The reason the weaker NRL lights are more effective is that the system in the chamber did not produce sufficient radiation below about 310 nm where $O(^1D)$ and hence OH is formed. The NRL lamps were not used in cloud processing experiments for fear of water damage.

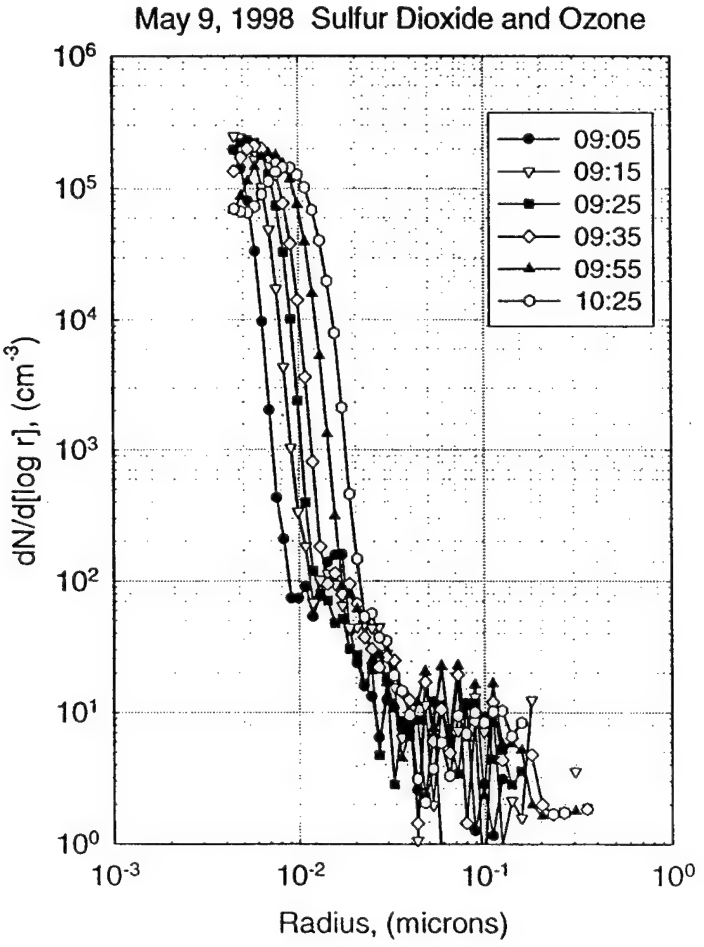

Fig. 22 – Nucleation and growth of sulfuric acid seed nuclei into a size range suitable for cloud processing. When the size distribution falls below about 20 to 30 cm^{-3}, the value is below the detection limit and is therefore zero.

Another alternative for producing seed aerosol is with the TSI nebulizer which is discussed elsewhere.

SO_2 Oxidation by O_3 during Cloud Processing

Data on SO_2 oxidation by O_3 during cloud processing was obtained on 8 and 12 May. We have only analyzed the data of 8 May. Fig. 23 shows the temporal plot of several of the measured parameters. The chamber was pressurized to about 21 mbar from about 14:57 to 15:09 as shown by the dashed line in Fig. 23. During the pressurized period at about 15:00, ozone was added to the chamber to increase the concentration from less than 20 ppb to about 80 ppb and SO_2 was added which increased the concentration to about 2 ppb by measurement. Actually enough SO_2 was added to increase the concentration to 5 ppb had there been no wall loss or loss to the water in the chamber. Unfortunately by this time the NRL TECO 43S had failed and the Canadian Environmental Services' TECO 43S had not yet arrived. The SO_2 data shown here was taken with a TECO 43A which is an order of magnitude less sensitive than the 43S (1 ppb rather than 0.1 ppb sensitivity). The expansion and subsequent cloud formation took place between 15:09 and 15:16. The aerosol mass (measured with the DMA at about 20% RH) shown by the solid circles increased from about 0.19 before cloud processing to 0.81 $\mu g\ m^{-3}$ after the cloud. Since the DMA scan requires about 4.5 minutes, several of the size distributions were partly in the cloud - these were not used in the calculation of mass conversion of 0.62 $\mu g\ m^{-3}$ (all calculated aerosol masses in this report assume unit density and therefore are in volume equivalence).

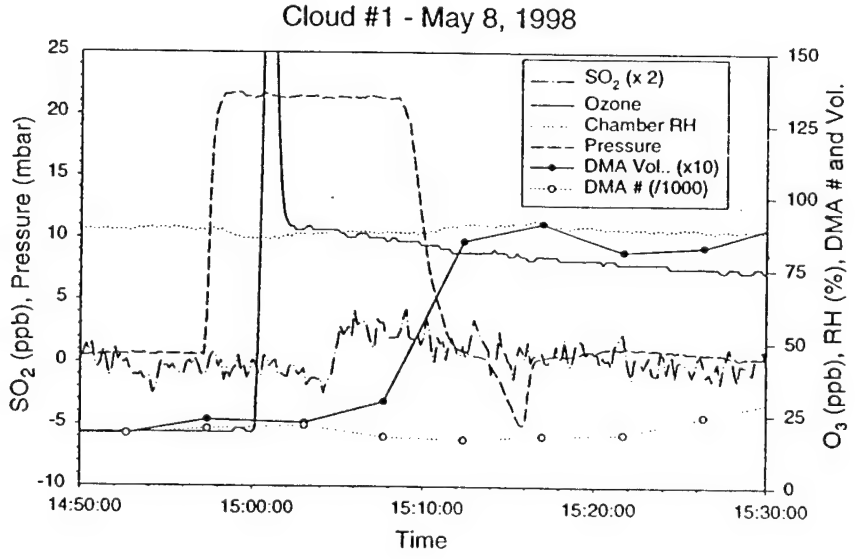

Fig. 23 – Temporal Plot of measured parameters during Cloud #1

Fig. 24 shows the size distribution before and after the cloud, together with the cloud droplet spectrum that peaks at 6 μm. The increase in the size of the particles that had been cloud processed is dramatic, and has a peak at about 0.11 μm.

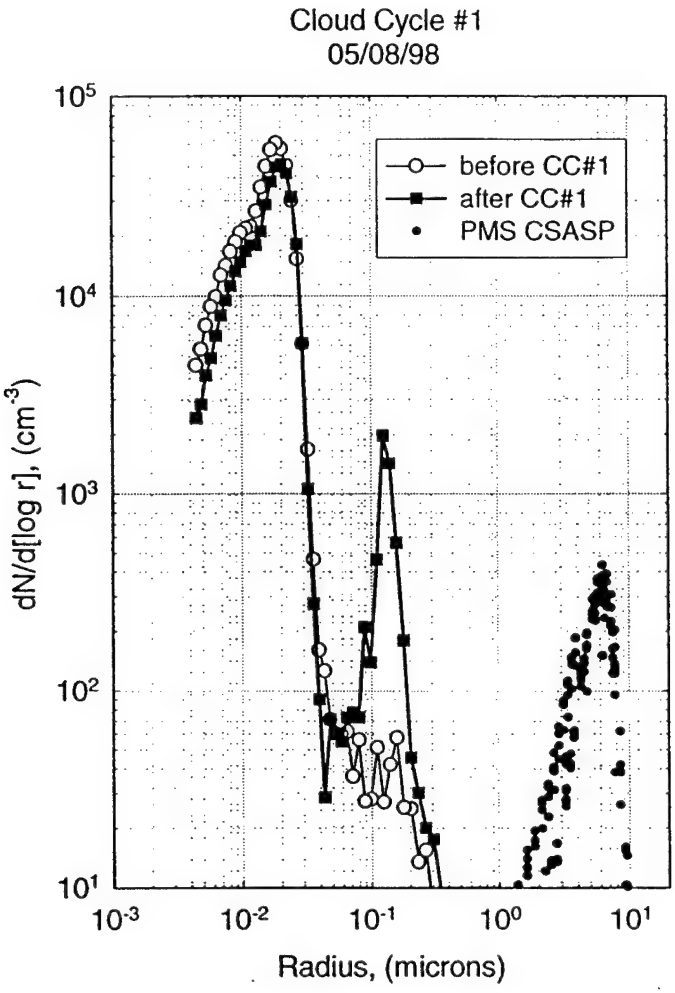

Fig. 24 – Change in the size distribution during first cloud cycle .

The result of the second cloud cycle is shown in Figs. 25 and 26. The expansion in this case also utilized the 2" ball valve that was opened during the initial phase of the expansion. SO_2 was added during the compression phase; no additional ozone was added. The faster expansion activated additional particles, produced slightly smaller cloud droplets, and produced the second hump on the cloud processed mode with hardly any change in the mode produced by the first cloud cycle. As in the past, we interpret this result to indicate that the residual acidity in the cloud droplets formed on the prior cloud-processed mode was sufficient to discourage additional reaction in these droplets. In those cloud droplets formed on the smaller particles not activated in the prior cloud cycle, the acidity was low enough so that the O_3-SO_2 reaction proceeded rapidly until the residual aerosol reached the radius of the peak occurring at the smaller radii. The trailing mode did not grow as large as the aerosol processed by the first cloud because the cloud droplets were somewhat smaller giving rise to the same acidity in the smaller drops of the second cloud as in the larger droplets in the first cloud. The number of cloud droplets measured with the PMS in the first cloud was about 91 cm^{-3} whereas the number in the second cloud was 173 cm^{-3} and the calculated LW was about 0.12 and 0.18 g m^{-3}. The numbers of cloud droplets by the cloud processing mode are 224 and 400 cm^{-3}, about twice that measured with the PMS. Likewise the IR measured liquid water was 0.25 and 0.255 g m^{-3}, about twice that measured by the PMS. This together with the predicted

LW starting from the point in time when the cloud first appeared makes us conclude that the PMS undercounted the cloud droplets by about a factor of two.

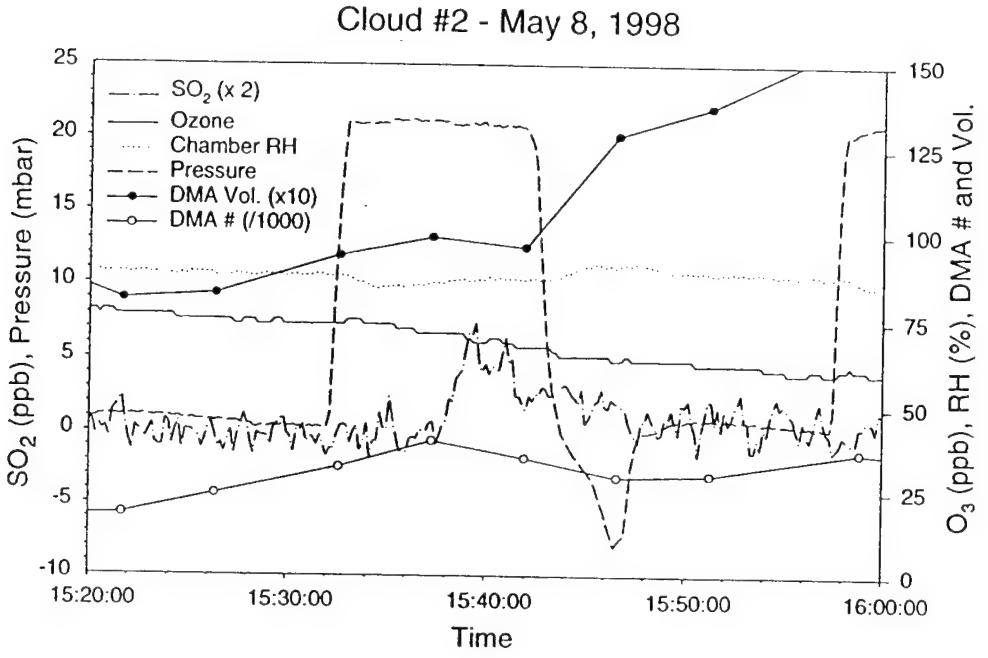

Fig. 25 – Temporal plot of measured parameters during second cloud cycle

A third expansion, slightly slower but with a slightly larger total expansion, activated the aerosol in both humps of the cloud processed mode. During the third cloud cycle the particles in the smaller hump grew, overtook, and joined the particles in the larger hump to form a single hump at the size of the larger size hump. This result, not shown, is explained by the fact that cloud droplets formed on particles in the trailing hump were less acidic and grew to have the same acidity as that provided by particles in the leading hump (hump at larger radius).

It was clear that further cloud processing would produce no significant aerosol mass by repeating any of the three prior expansions. We then decided to add about 10 ppb NH_3 to the system to neutralize the acid prior to the start of the compression cycle so that further conversion could be observed. The 10 ppb was calculated assuming no loss to walls or water in the chamber; in reality we expect all the injected NH_3 to end up in the water or used to partially neutralize the acid in the system. After compression we injected about 5 ppb of SO_2 which never registered on the TECO 43A which would have easily seen 1 ppb. We assume most of this SO_2 was absorbed on the walls or aerosols, or went into the water on the floor. Then within two minutes of cloud formation we added another 10 ppb of NH_3 (by calculation). The NH_3 would be expected to disappear rapidly to the water in the chamber. The change during the fourth cloud cycle is shown in Fig. 27. The decreased acidity caused by the added NH_3 resulted in a large increase in the radius of the cloud processed mode and a mass increase of 2.2 $\mu g\ m^{-3}$. It is clear that NH_3 has the predicted effect of increasing the SO_2 - O_3 reaction. However, there was no measurement of NH_3, so that it is not worthwhile to pursue this case further. It is imperative that we have measurements of NH_3 if we wish to pursue the effect of NH_3 on SO_2-O_3 oxidation.

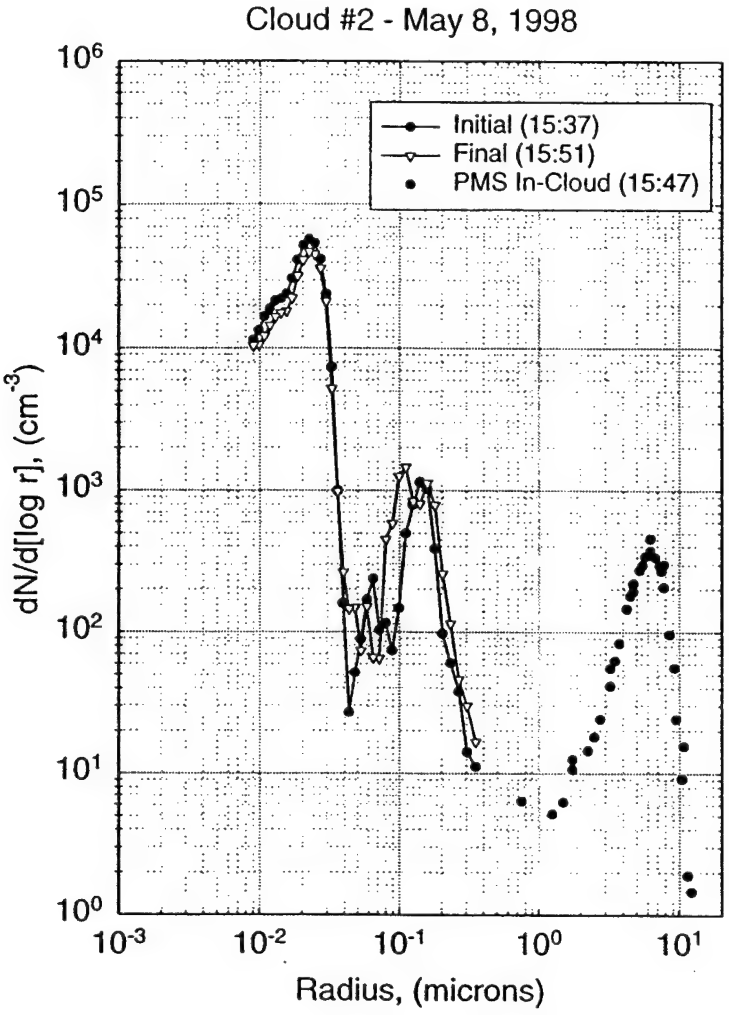

Fig. 26 – Change in the size distribution during the second cloud cycle

The above qualitatively demonstrates the pH dependence predicted by Hoffman's formulation of the O_3-SO_2 oxidation. This is not new; we did the same demonstration earlier (Hoppel *et al.*, (1994)). However when we made a quantitative comparison we found (mass) conversion rates 2 to 4 times greater than predicted by theory. In our earlier work we showed that Hoffman's expression could be used to derive the approximate relationship between the radius, r, of the processed aerosol and the radius of the cloud droplet, R:

$$\frac{r}{R} = [(\frac{r_o}{R})^9 + 3.93X10^{-5} P_O P_S t]^{1/9} = 0.324(P_O P_S t)^{1/9}$$

where P_O and P_S are the ozone and sulfur dioxide concentrations and t is the time in seconds in the cloud. r_o is the radius of the CCN prior to cloud processing and the last term assumes the processed nuclei are much larger than the original nuclei. This expression indicates that the main parameter determining the final (dry) radius is the size of the cloud droplet. The dependence on the ozone and sulfur dioxide concentration and time is quite weak, i.e., errors in the exact values of ozone, sulfur dioxide, and time are

not nearly as devastating as errors in our knowledge of R, the cloud droplet radius. This expression somewhat overestimates this ratio because it neglects the acidity due to S(IV), includes only the acidity due to S(VI), and includes only the reaction of ozone with $SO_3^=$. In our prior experiments the observed ratios were about 40% to 60% greater than those predicted by theory, or in terms of mass, 2.7 to 4 times as great. These same order of magnitude discrepancies (but somewhat larger) were also found by more rigorous modeling effort.

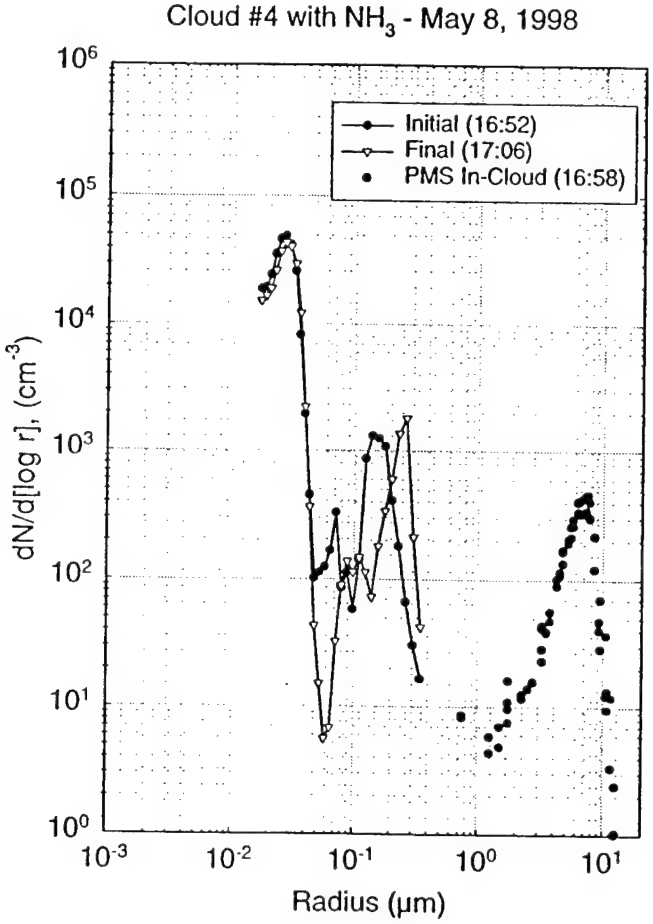

Fig. 27 – Cloud processing with NH_3 in the chamber

We have not had time to analyze this new data in detail but preliminary analysis of the peaks and concentrations of the reactants would indicate that we are observing the same conversion rates as we did before! Last time we attributed the difference either to the failure of the theory to describe the disperse state or possible contaminants in the chamber. If it were contaminants, we speculated it might be from out-gassing of the walls that were re-coated four month prior to the 1989 experiment or from the O_3 generator. We were very reluctant to suggest a problem with such an established theory. It has now been nine years since the walls were re-coated, and the observed conversion rate appears to be the same as we observed before. Further experiments must be designed to either (1) convince the community that there may be a problem with the present theory, better yet, show what is wrong, or (2) to discover what contaminant we have in the chamber which gives rise to the higher conversion rates.

SO_2 Oxidation by H_2O_2 during Cloud Processing

The goals of this experiment were to (1) test the method of injecting H_2O_2 into the chamber, (2) see if we could measure H_2O_2 at low levels (1 ppb), (3) see if an observable amount (>1ppb) of H_2O_2 could be maintained in the chamber against loss to the wet walls of the chamber, and (4) see if we could observe and quantify the in-cloud conversion.

H_2O_2 Injection Method

Hydrogen peroxide reactant gas was added to the chamber by flowing research grade N_2 at 2.0 liter min^{-1} over a bath of 50% H_2O_2 heated to approximately 50°C. The peroxide solution was contained in a 2-chamber, 5 cm diameter glass tube with a total H_2O_2 surface area of ~340 cm^2, and was suspended in a temperature-controlled water bath. The H_2O_2 vapor-containing N_2 was diluted with a second flow of heated N_2 (at 5 L min^{-1}) to prevent condensation of the peroxide/H_2O mixture in the injection line.

Injection rates as determined from the chamber concentration measurements described in the next section ranged from 0.9 to 1.3 ppbv min^{-1} to the dry chamber. After chamber humidification, injection rates ranged from 0.23 - 0.29 ppbv min^{-1}, owing to absorption of the peroxide into the water coating the walls and collected on the floor of the chamber. Additionally, a 30 minute delay between the start of the injection and detection in the chamber was seen in both experiments run (9 and 15 May). Condensation in the outlet of the peroxide chamber before mixing with the dilution gas may have been responsible, and this effect will be minimized in the Fall by reconfiguration of this line.

H_2O_2 saturated air flowing at 2 L min^{-1} would introduce ~10 ppbv min^{-1}, and thus by extension possibly >2 ppbv min^{-1} to the wet chamber. While these rates were not achieved in this experiment, injection rates were sufficient, and faster injection rates are possible simply by increasing the temperature of the water bath (i.e., a 10°C increase would increase the vapor pressure of peroxide by a factor of 1.8).

H_2O_2 Measurement Method

The concentration of hydrogen peroxide in the chamber was measured using a tunable diode laser absorption system designed for tropospheric atmospheric monitoring (Unisearch Associates, Inc., TAMS-150). This apparatus has previously been used in field experiments with an estimated overall accuracy of ±20% (See for example G.I. Mackay *et al.* (1996).) A brief description of the apparatus is given here.

The cryogenically cooled tunable lead-salt laser diode selected for this experiment emits radiation in many monochromatic and near-monochromatic modes in the 8 μm region, which overlaps with the ν_6 fundamental band of H_2O_2. Tuning is accomplished by varying either the diode temperature or the current to the diode. A monochromatic mode near 1260 cm^{-1} that is relatively free from overlap with water lines was chosen. The narrow line width of the tunable diode laser permits high selectivity, using fine adjustment of the diode current and temperature to obtain an absorption signal at a single ro-vibrational line in the H_2O_2 spectrum. The wavelength of the laser is locked to this line using software control of the temperature of the diode laser.

The radiation from the diode laser passes through a 1.5 m multipass absorption cell, making 96 passes for a total path length of 144 m. Pressure inside the cell is kept at 25 Torr, to reduce pressure broadening of the absorption line. The radiation is measured with a HgCdTe detector. The system is operated in the frequency modulation mode. The detector output is measured at the first harmonic of the modulation frequency, 2f, to increase the sensitivity.

Air enters the system through 0.25 inch PFA Teflon tubing located ~1/2 m inside the cloud chamber. A 2 μm pore size Teflon filter is mounted just outside the chamber to keep particulates out of the multipass cell. Air inside this tubing and filter is at ambient temperature and pressure. It then goes through a control unit consisting of a PFA Teflon solenoid valve that permits the ambient air to pass through a charcoal scrubber for background measurements or to pass directly through a Teflon needle valve, which was set to maintain a flow of ~5 slm, into the multipass cell. The control unit is heated to just above ambient temperature to prevent condensation in the lines. The valve is connected to the cell using ~5 m of 0.25 inch Teflon tubing. A motorized throttle valve mounted on the exit of the multipass cell is used to maintain the pressure at 25 Torr. Measurements are made by alternating background and ambient air measurements, averaging signals for 1 min. By subtracting alternate backgrounds from the ambient signal, minimum detectable limits of better than 1 ppbv are measured.

The system is calibrated by introducing a known concentration of gas-phase H_2O_2 at the inlet. The H_2O_2 standard is produced using a permeation device. In these studies, the output of the permeation device was measured both before and after each experiment, using the colorimetric $TiCl_4$ method to determine the flow rate of the H_2O_2.

Results of H_2O_2 Measurements on 9 May

When the H_2O_2 was injected into the chamber, a period of 0.5 h was required before it was detected at levels above 1 ppbv. The H_2O_2 signal rose to 29 ppbv before the water was added. The signal then rapidly dropped to ~1 ppbv. At the time of the first cloud expansion, the concentration of H_2O_2 was 1.02 ± 0.14 ppbv. At the time of the second cloud expansion, the concentration of H_2O_2 was 0.81 ± 0.08 ppbv. Water droplets were observed in the tubing exiting the chamber after the second cloud expansion, but it is not known when the condensation first occurred.

Results of H_2O_2 Measurements on 15 May

The results of the H_2O_2 concentration measurements are shown in Fig. 28. As can be seen, a passivation time was required before the H_2O_2 concentration reached a high level. As on May 9, the addition of water rapidly depleted the H_2O_2. At the time of the first cloud expansion, the concentration of H_2O_2 was 4.72 ± 0.18 ppbv. At the time of the second cloud expansion, the concentration of H_2O_2 was 4.75 ± 0.19 ppbv. During the next 2 hours, the H_2O_2 was added twice, as shown by the peaks in Figure V-7. At the time of the final cloud expansions, the concentration of H_2O_2 was 3.79 ± 0.14 ppbv. During these experiments, the tubing exiting the chamber was heated to slightly above ambient to prevent condensation in the line.

Results of Cloud Processing with SO_2 and H_2O_2

Only the results of the first cloud cycle on 9 May and 15 May were useful. The reason for this is that in the case of H_2O_2 oxidation of SO_2 there is no significant pH limitation to growth so that during the subsequent cloud cycles the processed particles grow beyond the size range covered by the DMA. Sizing with the OPC is not sufficiently accurate for calculation of mass conversion. For purposes of illustration we present only the result obtained on 9 May; the result of 15 May is similar.

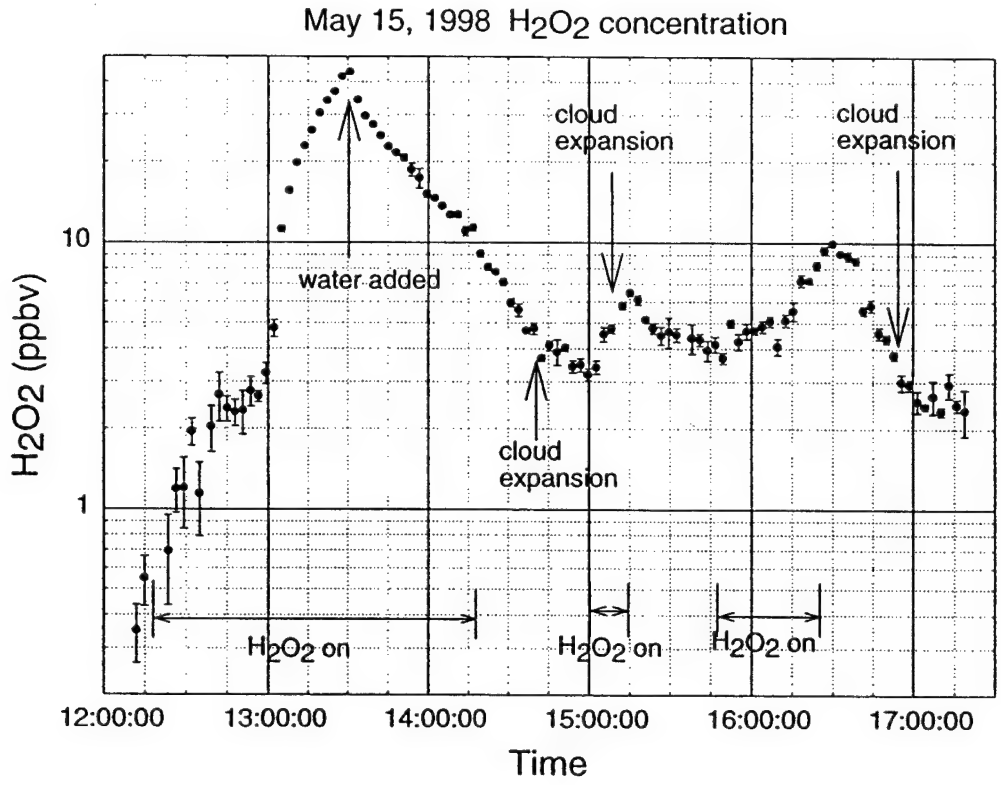

Fig. 28 – Hydrogen peroxide concentration

Fig. 29 shows the temporal change in the observations and Fig. 30 the change in the size distribution caused by the cloud processing. The volume increased from less than 0.1 μg m^{-3} (assuming

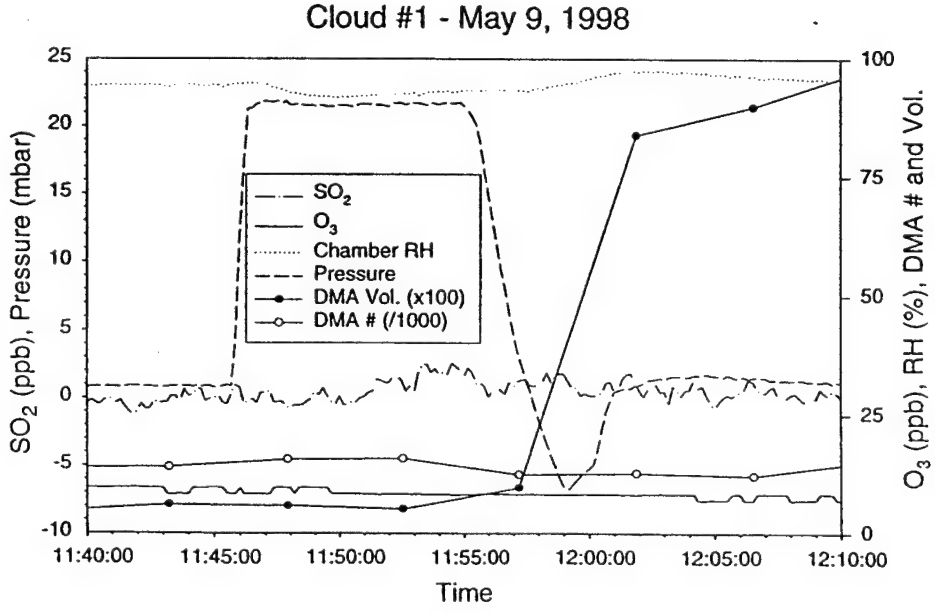

Fig.29 – Temporal change in observed parameters during the first cloud cycle on 9 May

unit density) to 0.88 μg m^{-3}. During the compression phase 5 ppb (by calculation) of SO_2 was added to the system but the actual gas-phase concentration increase was less than 1 ppb, the sensitivity of the TECO 43A. On the 19th when we had replaced the TECO 43A with a 43S, the increase observed when adding 5 ppb to a wet chamber was about 0.5 ppb. The total aerosol concentration remained nearly constant as shown by the open circles. The number of cloud droplets was 65 cm^{-3} and the liquid water content of the cloud was only 0.132 g m^{-3} (PMS). This small value of liquid water was caused by our inability to get the relative humidity near saturation as is discussed elsewhere. Most of the expansion was used just to obtain saturation. As is evident from Fig. 30, the aerosol droplets grew to the largest size measurable by the DMA. The DMA looses accuracy when the number of particles does not fall off rapidly in the largest channels. The reason for this is that in the data inversion scheme the number of larger particles must either be negligible or be known to correct for larger, multiply-charged particles which cannot be distinguished from smaller, singly-charged particles.

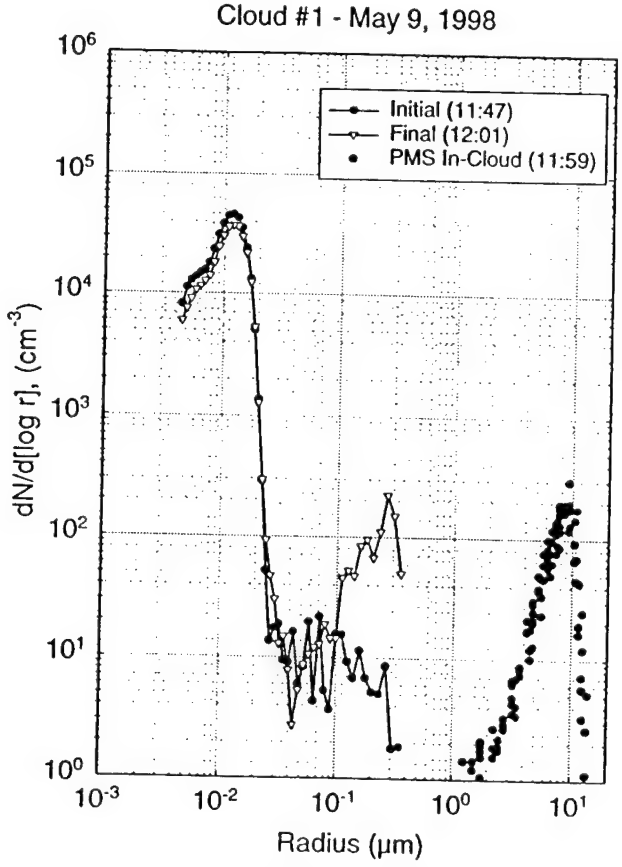

Fig. 30 – Change in the size distribution during Cloud Cycle #1 with H_2O_2 and O_3

Cloud Processing of Hydrocarbons

On one occasion we did cloud processing with cyclopentene and ozone in the chamber. We saw a definite but small cloud-processing signature. Since the cyclopentene reaction with ozone in the gas phase is so fast as demonstrated in the next section, it is difficult to see how the cloud processing conversion could be of atmospheric importance compared to the gas phase conversion. Nevertheless this is an experiment which could be pursued. We did not have time to try cloud processing on any other HC.

Cloud Processing in a Clean Chamber

Generally we see no observable cloud processing signature in a clean chamber with no SO_2. For example on one occasion we turned the chamber lights on and waited for particles to grow in. As shown in Section II, if the chamber lights are turned on in the clean chamber, there is a slow formation and growth of particles. These particles were used as seed nuclei on which to form a cloud. We saw no cloud processing signature in this case.

However we obtained a disturbing result when we produced ammonium sulfate seed nuclei by nebulizing ammonium sulfate solution in the clean chamber. The size distribution of ammonium sulfate is that shown in Fig. 21 and was produced by nebulizing a few cubic centimeters of ammonium sulfate solution, prepared by dissolving 6.1 mg of ammonium sulfate per liter of triply distilled water, into the chamber using reagent grade Nitrogen gas as the carrier. In this case when we did a cloud cycle prior to adding other reactants, we saw a small but distinct cloud processing signature. (Small compared to prior cloud-processing signatures shown in this section.) We can only surmise that the evaporation of the ammonium sulfate solution droplets during nebulization produced some ammonia and/or gaseous sulfur compound that showed up as liquid-phase reactants during the cloud processing.

Summary and Recommendations

Cloud processing is the most demanding procedure that will be executed in the chamber, both in regard to the chamber condition and on the operating personnel. The chamber is in better condition than in 1990 with respect to leaks in the air handling system and the refurbished long path IR measurement of liquid water seems to be in good working order. The measurement of the cloud liquid water is crucial because the PMS-OPC cannot measure liquid water with sufficient accuracy. While the OPC can measure the droplet size spectrum, the measurement of absolute numbers is not very accurate. Uncertainties in sensing volume, air flow rate, and collection efficiency through the horn accumulate to make the absolute value of LW less than desired in these experiments. The size distribution measured with the OPC can be normalized by the IR liquid water measurement. As a backup we also have the Gerber LW meter.

Recommendations

1. CUBRC has suggested that they can further improve the tightness of the air handling system and will do so before the Fall deployment. We heartily endorse this effort. During the 10 minute compression phase preceding cloud formation, any air lost to leaks must be made up. While this make-up air comes through the filtering system, it is not representative of the air in the chamber with regard to reactants and humidity. In fact, the make up air may be part of the reason that we were not able to get the dew point depression as low as we would have liked prior to cloud processing.

2. The venting system for making the cloud expansion is not adequate for all desired cloud expansions. The (manually operated) valve is too small for the fastest expansion desired and there is no quantitative measure of the flow rate except the chamber pressure. CUBRC has agreed to install a larger valve and possibly design a meter to monitor the volume flow rate out of the chamber. The latter would give a measure of dp/dt that is more relevant when trying to control the expansion rate.

3. On this occasion we were not able to get the dew point depression as small as we had during our prior visit to the chamber, which took place in the Fall of the year. We suspect that the floor of the chamber may have been colder than the walls and ceiling. Since water puddles on the floor of the chamber during humidification, the temperature of the water on the floor is probably the major determinant of

water vapor pressure in the chamber. To remedy this CUBRC has suggested that they install temperature sensors in the floor, wall, and ceiling to monitor any differences and install a heater in the crawl space under the chamber, which is a labyrinth of steel girders. We recommend this definitely be done before the Fall experiments. This will shorten the time to humidify the chamber, as well as provide a saturated (or nearly so) chamber at the start of the expansion giving higher liquid water for the same expansion.

4. The liquid phase chemists need to evaluate these experiments in light of the measurements we have available and decide if we have sufficient measurement diagnostics to bring closure to the experiments. If we plan to include NH_3 in the SO_2-O_3 experiments, we certainly need a measurement of NH_3. We need to know for certain if Aerodyne will be able to measure NH_3 with one of their chemical ionization mass spectrometers (CIMS) and if not, find someone who can add this capability.

The liquid-phase diagnostics are particularly troublesome since NSF did not fund the joint proposal by the Naval Academy and the University of Rhode Island, which were intended to be the mainstay of the liquid-phase chemistry experiments.

VI. PHOTOLYSIS OF DIMETHYL SULFIDE (AND SO_2)

On 20 May, 30 ppb of DMS were injected into a clean chamber at about 09:05. From 09:05 until 11:26 the chamber was monitored and five GCFI samples were taken to see if any wall loss of DMS could be detected. During this period there was no particle formation. At 11:27, about 110 ppb of O_3 was injected into the (dark) chamber. Within a few minutes ultra-fine particle production was observed by the ultra-fine CNC and after about five minutes these particles had grown into the range detectable by the TSI 3022 CNC, as can been seen in Fig. 31. They weren't detectable in the DMA ($r>0.005$ μm) until after 30 minutes had passed. Even though the nucleation rate was high the growth rate was slow. The ultra-fine CN concentration was off scale at 10^5 cm^{-3} but came back on scale at about 12:10 as nucleation subsided and particle concentration was reduced by wall losses and coagulation. At 12:22 the (NRL) UV lights (λ=254nm) were turned on. After the UV lights were turned on, the ultra-fine CNC concentration again went off scale and shortly thereafter the CN concentration increased from about 45K to 90K cm^{-3} over the next 20 minutes. This indicated that after the lights were turned on the nonvolatile reaction product (probably H_2SO_4) increased, nucleation occurred, and these particles slowly grew into the detectable range. This could be seen a few minutes later in the DMA size distribution as a new hump (trailing mode) appeared in the smallest DMA channels. The aerosol mass continued to increase even after the concentration begin to fall after about 12:50 and the second mode grew well within the range of the DMA size measurement. There was an increase in the SO_2 concentration from about 0.2 ppb (instrument zero) to about 1.5 ppb (scale in Fig. 31 is linear for SO_2), an increase of more than 1 ppb. Unfortunately we had no measurement of DMS or other end products during the photolysis experiment. However, these capabilities are planned for the main experiments.

In a prior deployment to the Calspan Chamber we saw no detectable SO_2 in the chamber and no significant aerosol mass formation when O_3 (and DMS) was irradiated by the chamber's irradiation system. We take this as an indication that the chamber lights did not go to a short enough wavelengths to produce significant amounts of OH to observe DMS oxidation.

We speculate that if nucleation here is due to H_2SO_4 as seems probable, and if we had a measure of H_2SO_4 vapor concentration as we will have for the second phase experiment, then nucleation rates could be calculated for both nucleation events. However the second nucleation event (about 12:25) might give a more sensitive indication of nucleation, because nucleation rates would be slower and H_2SO_4 concentrations smaller; i.e. you would be closer to the (detection) threshold for nucleation.

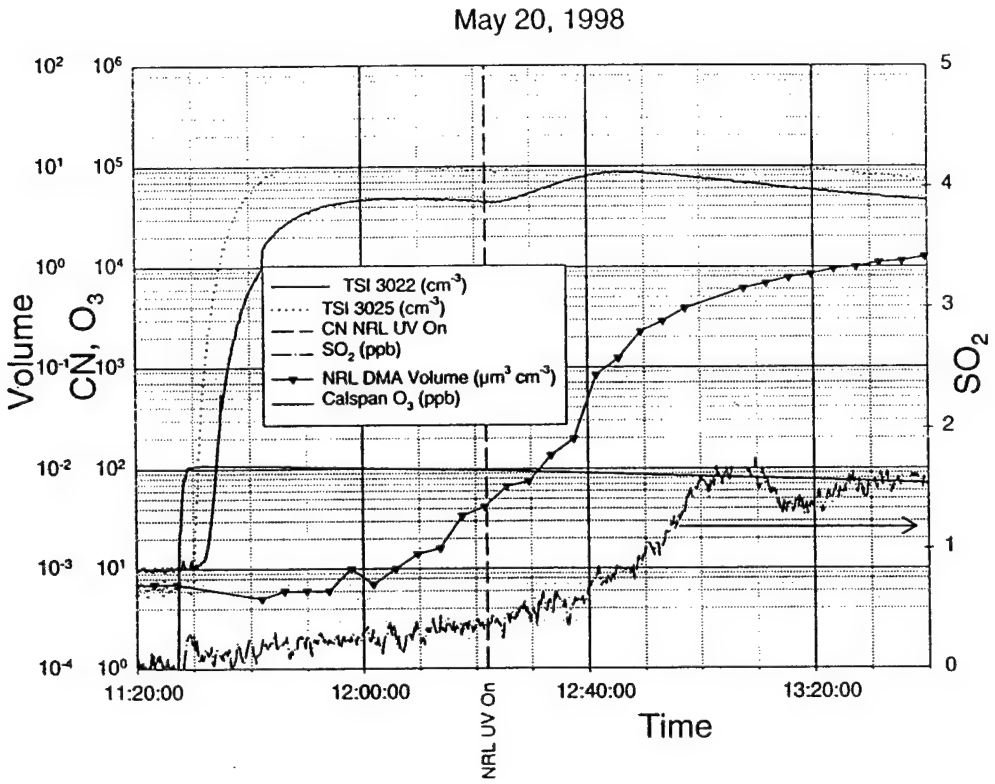

Fig. 31 – Aerosol formation during photolysis of DMS in concentration of about 30 ppb

Summary and Recommendations

This experiment was done on the next to last day of the deployment. It was delayed to allow Calspan time to demonstrate that they could detect DMS with their GCFI system. It was not possible to test the DMS photolysis experiments to the same degree that we tested other proposed experiments because the DMS experiments rely more heavily on measurement technologies that were not available during the characterization experiments. We need other participants to carefully evaluate the adequacy of the resources available and see if they are sufficient to make a contribution beyond what has already been made, and to identify any shortcomings in resources and suggest solutions. The following are of concern.

1. We assume here that oxidation of DMS will be by OH produced from photolysis of O_3. Using this scheme to produce OH can keep the system free of NO_x, which greatly complicates the picture. We may want to limit our study to the low NO_x environment (such as the remote marine environment). We did demonstrate that for 30 ppb DMS photolysis of 100 ppb of ozone with the NRL portable UV lamps produced small but measurable aerosol mass and SO_2 concentration (Fig. 31). The wavelength of these lamps was 254 nm and the observed results were probably due to OH produced by photolysis of ozone. However, unlike the chamber irradiation system, the intensity and spatial distribution of the radiation of these portable lamps has not been characterized. The mixing fan does keep the chamber well mixed on a time scale of less than a minute, so that any reaction that takes place on the order of a minute or less can probably be considered to be occurring in a uniformly mixed chamber. Also Calspan has volunteered to install and test UV lamps constructed from spare FS-40 UV lamps which they have. These added lamps would not be behind the existing lamp windows which block radiation

below 310 nm (see Fig. 6 for spectral characterization). We need some atmospheric photochemist to address this issue and give us advice quickly so that the necessary preparations can be made.

2. We need a faster measurement if DMS depletion than is currently provided by the GCFI (20 min sample). Aerodyne has said they will try to measure DMS, DMSO and $DMSO_2$ with a positive ion CIMS as well as the acids (negative ion CIMS). However it is not clear where we stand on this capability, as we enter the final stage of preparations.

If we have real time measurements of DMS, OH, HO2, H2SO4, MSA, DMSO, and DMSO2, as is possible under the best-case scenario, we will undoubtedly have the most complete data set on DMS photolysis that exists and under conditions that are fairly realistic and well defined.

VII. AEROSOL FORMATION BY REACTION OF O_3 WITH HYDROCARBONS

Aerosol formation caused by reaction of HCs with O_3 was observed for cyclohexene, cyclopentene and alpha-pinene. The experiments for the first and last of these HC's were carried out following the wall loss measurements in a clean chamber described in Section II.

Cyclohexene

In addition to wall loss measurements of cyclohexene given in Section II, we also irradiated cyclohexene using the chamber's irradiation system for thirty minutes and saw no aerosol production (no increase in ultrafine particles). We then turned off the lights and after a short time added about 120 ppb of O_3 to the (about) 50 ppb cyclohexene already in the chamber. Immediately large concentrations of ultrafine particles were detected with the ultrafine particle counter. Fig. 32 shows the number and mass

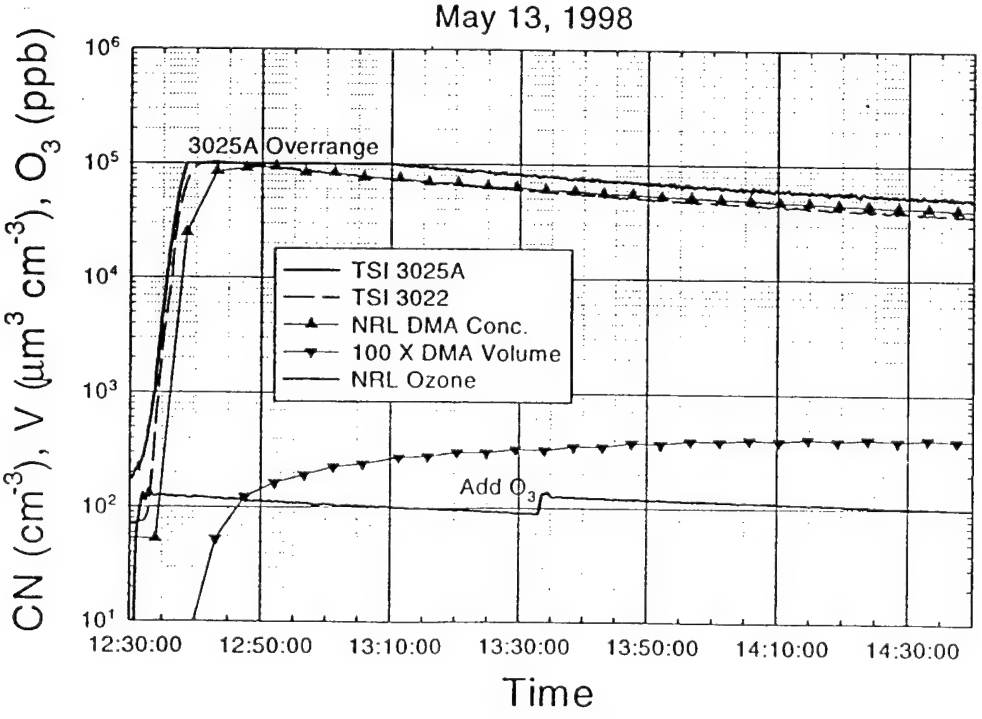

Fig. 32 – Aerosol production from Cyclohexene reaction with Ozone

concentration (as measured with the NRL DMA) as a function of time. The solid triangles indicate the number and mass as calculated from the aerosol size distribution measured with the NRL DMA about every five minutes. The agreement between the concentration measured with the TSI 3022 and calculated from the NRL DMA is remarkable after the particles had grown into the range of the DMA.

Fig. 33 shows the evolution of the size distribution. The growth into the DMA range is very rapid; much more rapid than were are used to seeing with O_3 and SO_2, in which case we assume the condensing product is H_2SO_4. Particularly striking is the smaller ratio of the number of particles nucleated to the growth time. This would indicate that the product being formed has a lower nucleation potential than H_2SO_4, but the yield of the condensing material is greater. However the mechanism for the later reaction (via Criegee intermediates) is entirely different and probably depends upon the background NMHC in the chamber so that comparison of the yields are not very meaningful.

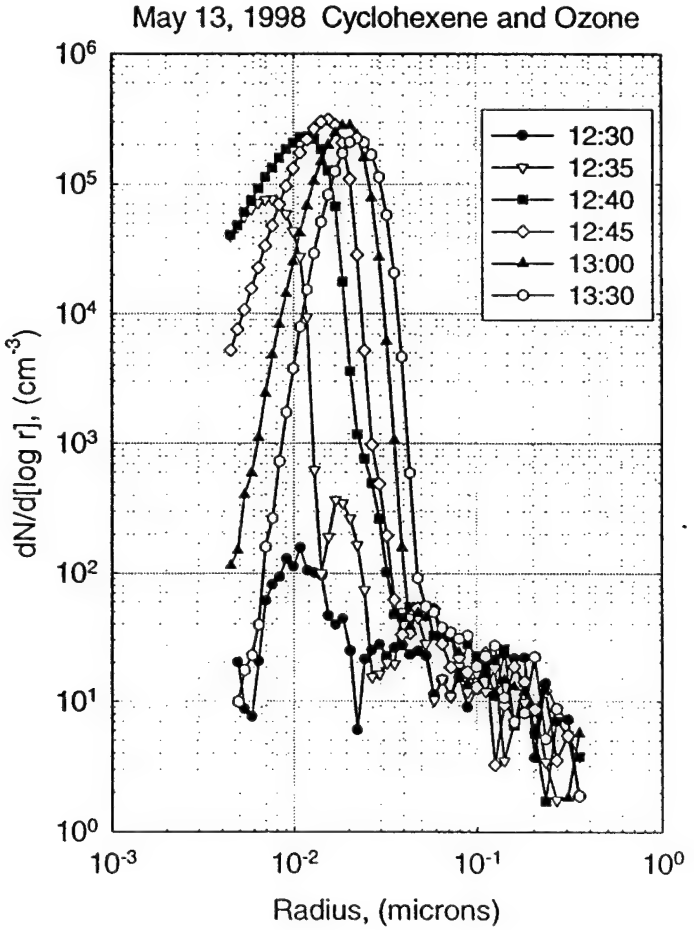

Fig. 33 – Successive size distribution measured during nucleation and growth of particles resulting from reaction of Cyclohexene with Ozone

Since we have no continuous measurement of the HC concentration, the leveling off of the aerosol mass concentration in the chamber exhibited in Fig. 19 could be attributed to either the

completion of the reaction or a balance between production and surface deposition to the walls of the chamber. The initial rate of mass production in the chamber is estimated from the data to be about $7X10^{-7}$ g s^{-1}. If we take the mass deposition velocity to be about 0.02 cm s^{-1}, as measured for the number deposition velocity in Section III, together with the asymptotic value of aerosol mass density in the chamber, we get a wall loss rate of $3X10^{-7}$. These two values are as close as we could expect for this kind of estimate and indicates a balance between production and wall loss. This is explored in more detail in the analysis later in this section.

Cyclopentene

Aerosol production from the reaction of cyclopentene was measured in similar fashion to that of cyclohexene. The only difference was that from the time of injection of cyclopentene in the chamber to the time of ozone injection was only about 30 minutes rather than 2 hours, as was the case for cyclohexene. Wall loss measurements for cyclohexene would indicate that any loss of cyclohexene during the extra 90 minutes would have been minimal. Fifty ppb was injected in both cases. The results for cyclopentene are shown in Figs. 34 and 35. Here the maximum concentration was a factor of two less, but the growth rate (mass formation) was much greater. (Note that the time scales on Fig. 32 and Fig. 35 are different.) Twenty minutes after injection of Cyclopentene the mass concentration was about 5 μg m^{-3} whereas for cyclohexene it was only about 1.3 μg m^{-3}. The above (less particles and faster growth) would indicate that the condensing product for the cyclopentene reaction had a greater yield but was more volatile (lower nucleation potential) than for the cyclohexene case.

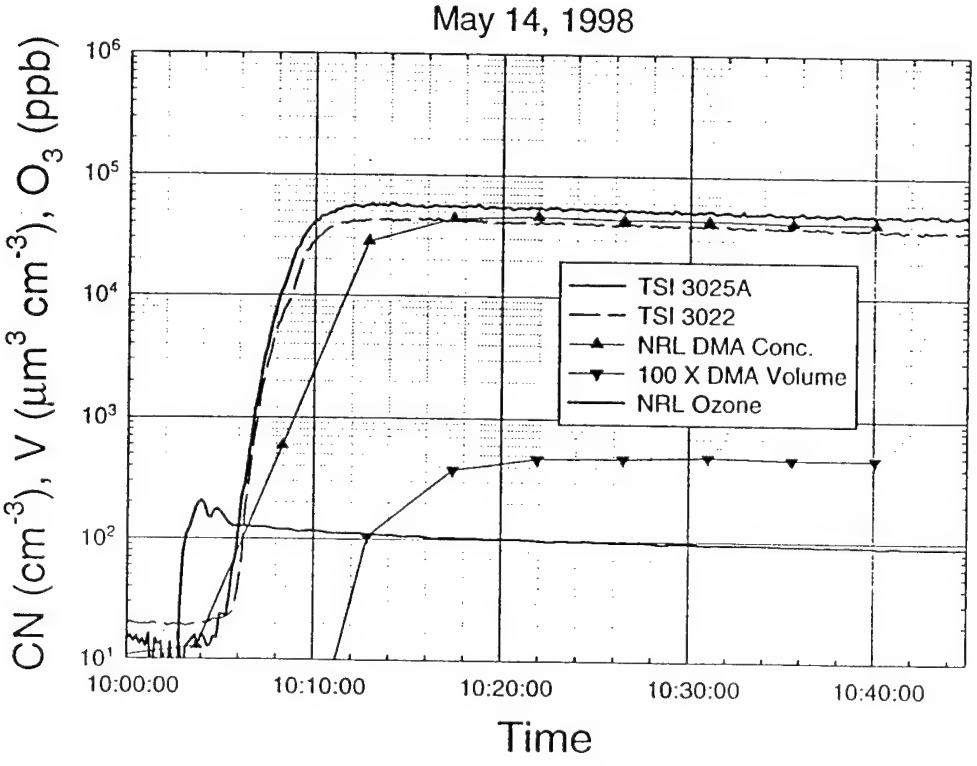

Fig 34 – Aerosol production from Cyclopentene reaction with Ozone

The rapid growth shows up even more dramatically in a plot of successive size distributions shown in Fig. 35. The first size distribution (solid circles) was before the injection of ozone and is at the noise level of the DMA.

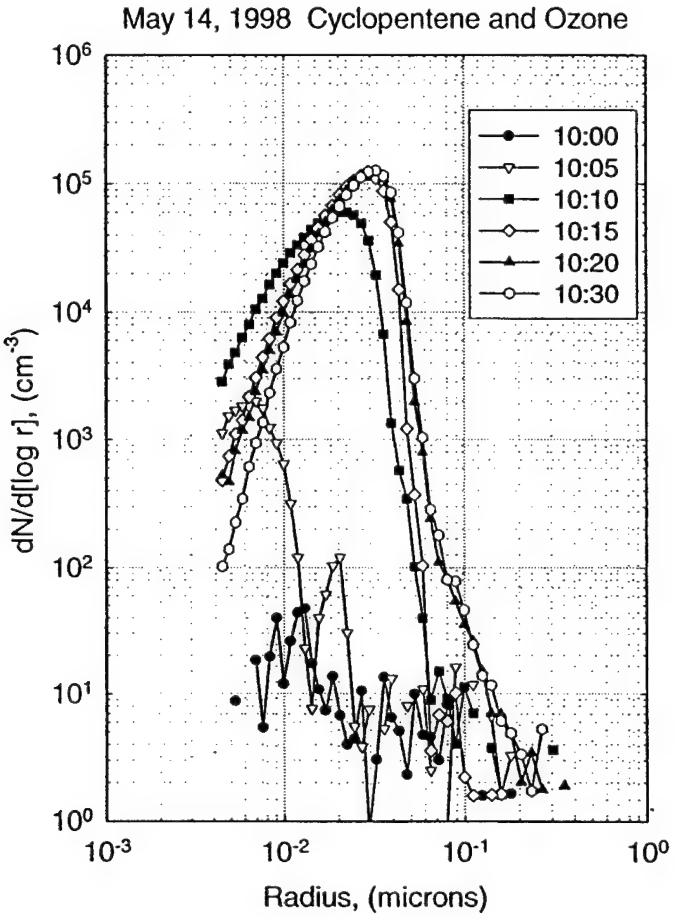

Fig. 35 – Successive size distribution measured during nucleation and growth of particles resulting from reaction of Cyclopentene with Ozone

Alpha-Pinene

Similar measurements were made with α-pinene. Alpha-pinene has a lower vapor pressure and the supplier of the α-pinene could not supply it at the concentrations ordered. In the mix-up that followed the amount ordered was only sufficient to inject 10 ppb into the (clean) chamber on 19 May. After two hours of monitoring to determine wall losses as described earlier, the chamber irradiation lights were turned on at 11:17 and off at 11:40 to see if irradiation of α-pinene would have any effect on aerosol formation. The irradiation produced particles and is the cause of the increase shown at the start of Fig. 36 in both the ultra-fine particles and CN measured with the TSI 3022. At 11:40, when the lights were turned

off, particle production ceased. During this time the particles never did grow large enough (r>0.005 μm) to show up in the DMA data. While the mass production (yield) was low, the number and speed at which the particles formed were clearly much greater than for photolysis of a clean chamber (Fig. 11) or for the case of cyclohexene where the same irradiation procedure produced no observable nucleation. We did not have time to pursue this further and introduced ozone (with lights off) at about 11:50 at a concentration of about 100 ppb. In less than five minutes particles appeared in the DMA size range (upright triangles in Fig. 36) and the mass increased to over 1 μg m^{-3} in ten minutes. It is difficult to conclude anything about the comparative yield without further analysis because of the lower concentration of α-pinene used here than in the case of the prior two HCs. However it is clear that the vapor pressure of the condensing reaction product is lower than for the case of cyclopentene; i.e., the product had a greater nucleation potential. While the lights alone (no O_3) did produce significant number of particles, the ozone at 110 ppb had a much greater effect.

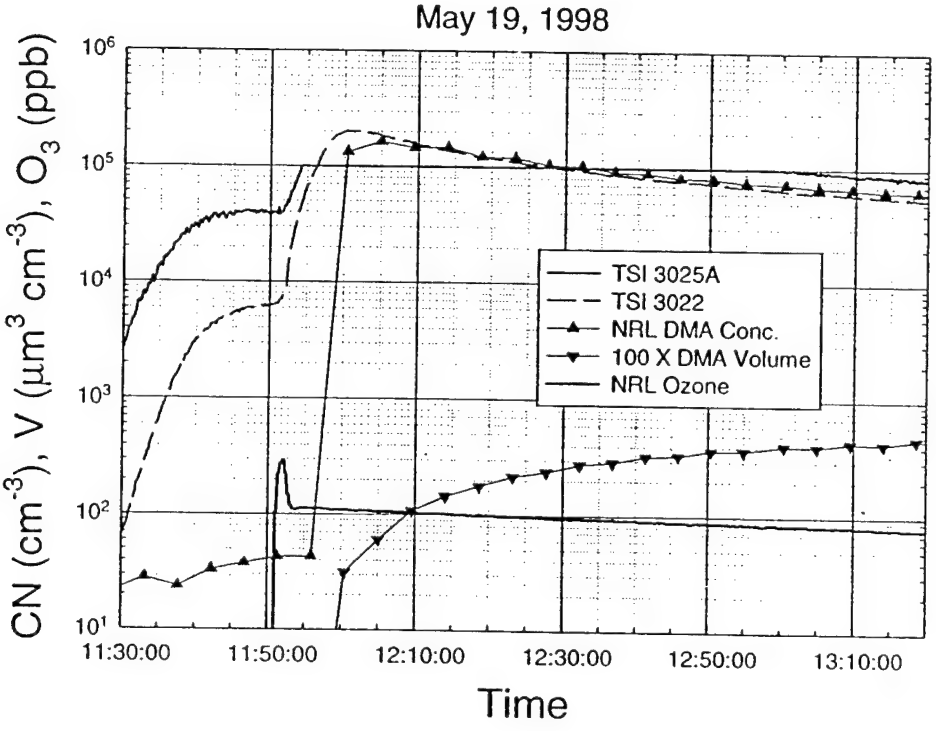

Fig. 36 – Aerosol production from alpha-pinene reaction with Ozone

The growth of the size distribution of the alpha-pinene is shown in Fig. 37.

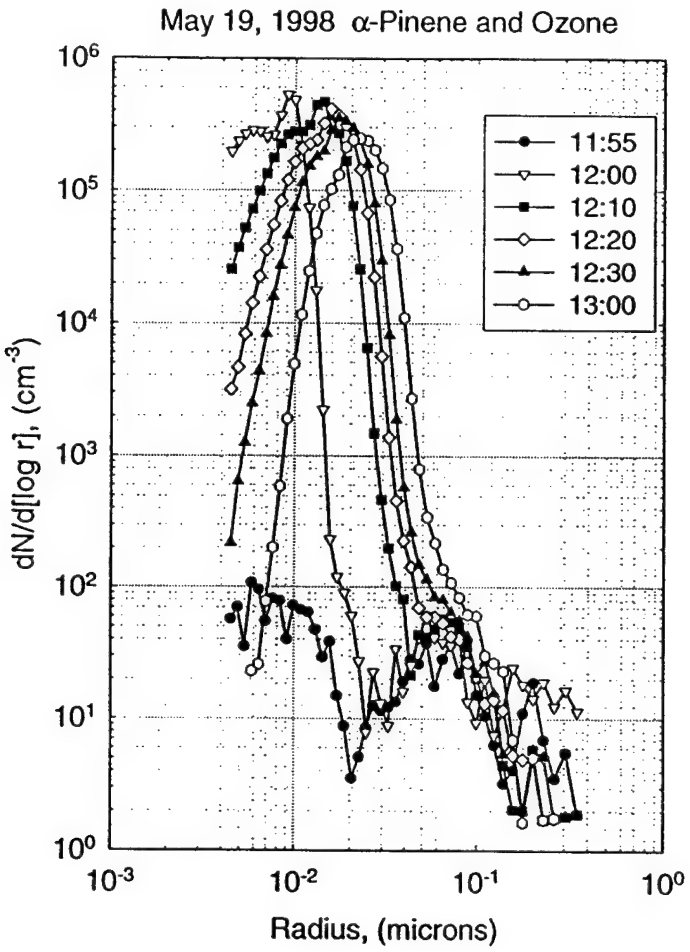

Fig. 37– Successive size distribution measured during nucleation and growth of particles resulting from reaction of alpha-pinene with Ozone

Comparison of the Hydrocarbons

To compare the effectiveness of the three HCs above for producing aerosol mass, we define a second order rate constant for mass production as:

$$k = \frac{1}{[O_3][HC]}\left(\frac{dM}{dt}\right)_{initial} \qquad (2)$$

where the concentrations of O_3 and HC and M are all expressed in mass per unit volume. We hasten to point out that we do not know what chemical reactions are taking place, nor the order of the reaction. The expression for k is just a means to normalize for different concentrations of reactants and compare, somewhat quantitatively, the effectiveness of the three HCs to produce aerosol mass. The values of k so obtained from Equation (2) are 1.42, 8.0 and 3.1 {$X10^{-6}$ m^3 $(\mu g)^{-1}$ min^{-1}} for cyclohexene, cyclopentene, and α-pinene, respectively. Clearly, by this measure, cyclopentene is about 2.5 times faster than α-pinene and over five times faster than cyclohexene.

Seinfeld and Pandis (1998) give total yields of aerosol mass from cyclohexene, cyclopentene and α-pinene as 278, 132, and 762 μg m^{-3} per 1 ppm reacted, respectively. Since we did not have a measure of the amount reacted we are not able to compare above rates with total reacted. It is interesting that k was the largest for cyclopentene, whereas the total particulate yield given in Seinfeld and Pandis is the lowest of the three for cyclopentene.

Simple Analysis of the Above Hydrocarbon Data

The following simple analysis may help the reader in understanding the behavior of the data shown in this section. After ozone is introduced onto the chamber it reacts rapidly with the HC to produce low-volatility product(s) whose concentration builds up to the concentration where nucleation of new particles takes place. This nucleation takes place in a burst that lasts several minutes, until sufficient aerosol surface area is generated to absorb the low-volatility product(s). These ultra-fine nuclei grow first into the size range detectable by the TSI 3025 CN counter, then into the range of the TSI 3022 and finally into the size range (r>0.005 μm) of the DMA size spectrometer, as the newly formed material condenses on the existing particles. The ratio of the number of particles formed to the growth time is loosely related to the vapor pressure of the product. For the same rate of product formation, the lower volatility product will nucleate many more particles, but produce about the same aerosol mass.

If we consider the evolution of the size distribution and mass after the nucleation phase is completed we can see how the aerosol number and growth interacts with the chamber parameters. Making the following assumptions greatly simplifies the analysis and still describes the essential behavior:

1. The particles are monodisperse (the observed size distribution is strongly peaked).
2. Coagulation is small compared to wall losses of monodisperse particles. (We saw earlier in Section III that this is true for monodisperse particles when the concentration is less than about 10^5 cm^{-3}.)
3. The particles are smaller than the molecular mean-free-path. (This assumption is not necessary for the analysis, but is valid for the particles considered here, r<0.03 μm, and simplifies the expressions.)

Since wall loss is the only loss for particles, the total concentration can be written as we did in Section III as

$$Z(t) = Z(0)\exp(-\lambda_{part}t) \qquad (3)$$

where Z(0) is the initial value after the nucleation phase is completed and $\lambda_{part.}$ was determined in Section III and given in Table 3.

The growth equation for a particle of radius r can be written as

$$\frac{dr}{dt} = \frac{\alpha \bar{v} m}{4\rho} N_{svp}\left(\frac{N(t)}{N_{svp}} - 1\right) \qquad (4)$$

where α is the condensation coefficient, $\bar{v}$ is the mean molecular velocity, m the mass of the condensing molecule, ρ the density of the condensing product, and N_{svp} is the saturation vapor pressure of the condensing material. Here we have neglected the Kelvin effect.

The concentration of the condensable vapor in molecules per unit volume is N(t), and given by

$$\frac{dN}{dt} = Q - \lambda_{vap} N - \alpha \pi v Z r^2 (N - N_{svp}) \qquad (5)$$

where Q is the production rate of N from the reaction of ozone and HC, λ_{vap} the wall loss constant for the vapor product, and the last term is the loss of vapor by condensation on aerosols.

We have solved these three equations for the cyclohexene case using the initial value of $Z(0) = 10^5$ as indicated in Fig. 32. The value of Q was also estimated from the initial mass increase from the same figure, assuming that wall loss of aerosol mass was negligible during the first twenty minutes (aerosol mass was still in the buildup stage). We further assumed that the condensing product was adipic acid with a SVP of 0.08 ppb as given in Seinfeld and Pandis (1998). Fig. 38 shows the solution as compared to the observations (shown in Fig. 32) during the first hour. The aerosol loss agrees well with that

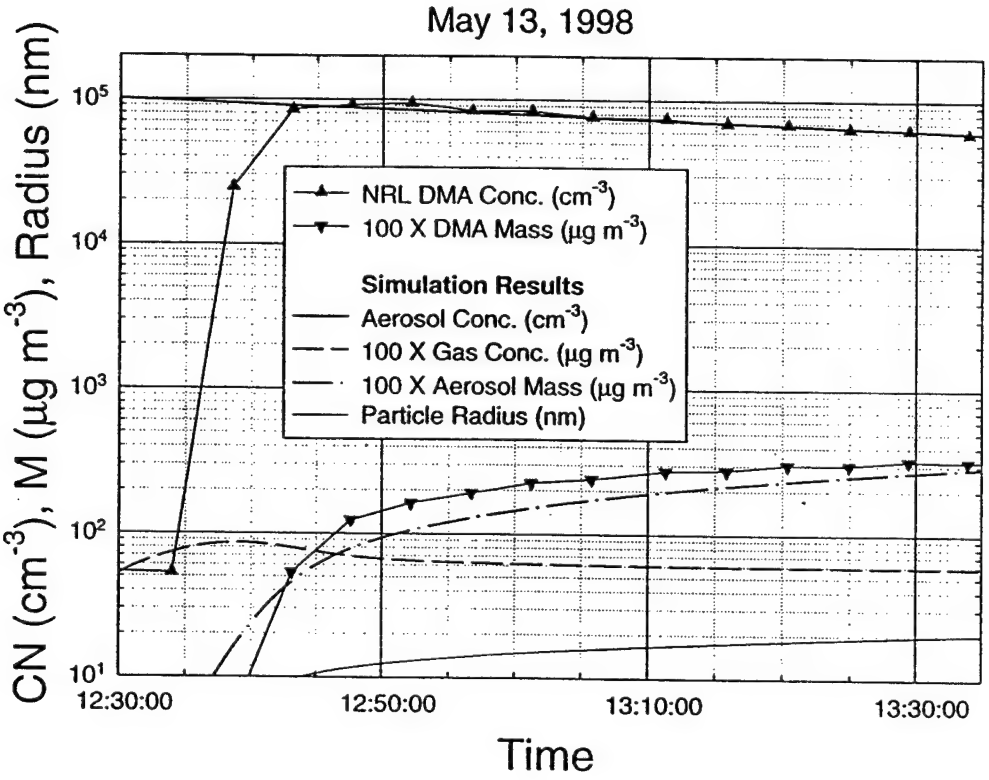

Fig. 38 – Comparison of simulation and data for cyclohexene

predicted by Equation 3 after nucleation has ceased. The growth of particles to a radius of 0.02 µm (20 nanometers) in one hour is also in agreement with observations of Fig. 33. The total aerosol mass after one hour is 2 µg m^{-3} in both cases, but the time constant for growth of mass is faster in the observations than in the simulation. However, the fast initial growth rate shown by the observation may well be an artifact because the DMA does not measure particles smaller than 0.005 µm. There is a decreasing

efficiency of particle detection, and increased diffusion loss at radii below about 0.008 μm radius as well as an increased time for the particles to come to charge equilibrium (necessary for accurate DMA measurement). Therefore we would expect the aerosol mass as measured with the DMA to increase more rapidly than is actually the case as the particles move within the range of greatest accuracy (r>0.008 μm) of the DMA. Also in the analysis we have assumed that λ_{part} is constant. This is not the case, ultrafine particles will have a faster deposition rate than will larger particles. Since the time constant for the mass to reach its equilibrium value in inversely proportional to the deposition velocity, the equilibrium will be approached faster than predicted by this simple analysis. Another consideration is that the production rate is assumed to be constant. If the production rate decreases due to reduction of the reactants, then the time constant will appear to be faster. The dashed line in Fig. 38 gives the vapor density of the condensing product. The vapor density started at the SVP value and increased about 80% (80% supersaturation with respect to pure adipic acid) before the aerosol sink was large enough to drop the vapor concentration back near the SVP (determined by the pressure at the particle surface).

More interesting than the above are the changes that occurs when we change parameters in the model.

1. Lacking the wall deposition velocity of adipic acid, we used that measured for SO_2 as a surrogate. Decreasing the value of the wall deposition made little difference in the solution, indicating that wall losses of vapor were small compared to condensation on the particles. Doubling the vapor wall deposition velocity had an observable effect, and increasing the deposition velocity by an order of magnitude completely turned off growth. Wall losses of vapors (which are proportional to the vapor concentration) lowered the vapor pressure below the SVP (here assumed to be that of adipic acid) and therefore the particles did not grow. It could easily be imagined that a condensing species would have a deposition velocity greater than that of SO_2, but of course, at some point the loss is diffusion limited even if the molecules stick with 100% efficiency.

2. Changing the condensation coefficient and the SVP has the same effect. While the SVP is the chief parameter in determining nucleation, it has little effect on the growth process. Lowering the SVP increased the supersaturation seen by the particles, but also lowered the vapor concentration in the chamber so that the growth remains about constant. This is best understood by realizing that the aerosol growth is determined by the production of material and the vapor concentration in the chamber adjusts so that condensation is equal to the production rate. The same is true for changes in the condensation coefficient. The caveat here is that this does not apply when the SVP is high enough that wall losses compete with condensation loss to the aerosol.

3. The steady-state aerosol mass in the chamber is determined by a balance between production of mass and wall loss. This assumes that the production rate, Q, is constant; i.e., no depletion of reactants. From mass conservation the steady state mass concentration is given by Q_m/λ_{part} where Q_m is the mass production rate (the product of the molecular production rate, Q, and molecular mass). This maximum value in the above example is only about 8 μg m^{-3}. The time constant with which this value is approached is roughly $(\lambda_{part.})^{-1}$ and is therefore of the order of 1-2 hours (or possibly less as discussed above). If measurements are made by taking filter samples of the aerosol, an upper limit for material available for analysis is obtained. The only way the concentrations can be increased is to go to much higher reactant concentrations, which will increase Q. However higher reactant concentrations take us further away from the situation where the chamber concentrations are the same order of magnitude of those found in the natural environment.

Summary and Recommendations

1. It appears that the chamber is an excellent facility to study the O_3-HC reactions, which are potentially important in the formation of particulate matter in the atmosphere.

2. For these studies to be useful, we will need continuous measurements of the HC concentration with time resolution adequate to deduce the reaction rate. Also important to understanding the mechanism would be the measurement of other gaseous products. During the characterization measurements Calspan developed GC methods to measured the primary HC and several expected reaction products as suggest by Dean Hegg. I do not know how successful the measurement of these gaseous products was, nor the adequacy of the accuracy or temporal resolution of the measurements to meet the needs of the experiment. It is necessary to evaluate the GC methods and measurements made by CUBRC during the characterization measurements and determine what needs to be done, if anything.

3. The University of Washington proposes to measure the reaction products which form particulate matter by taking a filter sample at the end the HC-ozone experiment and perhaps also sample(s) during the run. As shown above, aerosol mass loading is expected to be only a few micrograms per cubic meter. Therefore the analysis method must have a sensitivity the order of a micrograms, or less, of material per filter. The mass loading can be increased by increasing the concentration of reactants, but this makes the measurements less likely to be representative of what happens in the atmosphere.

4. Reactions between O_3 and alkenes have been observed to produce OH radicals with yields sometimes close to unity. For example cyclopentene is estimated to give an OH yield of 0.6 (Seinfeld and Pandis, 1998). Since in the Fall experiment we will have a direct measurement of OH (Cantrell), this may offer a unique opportunity to see what role OH plays in the oxidation of HCs and the size of the OH contribution from atmospheric HCs.

VIII. HETEROGENEOUS CHEMISTRY ON SEA-SALT PARTICLES

Sea salt particles deliquesce at high humidities and form aqueous solution droplets of high pH. SO_2 oxidation by ozone is known to proceed rapidly in high pH droplets. The objective of the process studies experiments is to study the above reaction in Calspan's Chamber by measuring the uptake of SO_2 and O_3 and the change in aerosol composition; the latter capability was not present during the characterization experiments.

Calculations indicate that it will not be possible to inject a sufficient load of aerosol in the chamber at one time to produce observable decrease in SO_2 concentration. It will therefore be necessary to produce a flux of sea-salt aerosol (alkalinity) into the chamber. It is estimated that the alkalinity in one liter of seawater (dispersed in the chamber) would reduce the SO_2 concentration by about 5 ppb. Therefore about one liter of seawater, or its equivalent in alkalinity, needs to be nebulized over the period of an experiment to obtain an easily detectable depletion of SO_2. The aerosol load, the residence time of the particles in the chamber, and the flux through the chamber depend on the generation rate and the deposition rate (which in turn depends on size and concentration of the aerosol in the chamber). The above statement represented our understanding prior to the characterization experiments. As will be shown below, the uptake of SO_2 in real seawater appears to be faster than indicated above.

The proposed experiment would introduce sea-salt aerosol into the chamber at a size where the lifetime against surface deposition is long compared to the reaction time. The oxidation of SO_2 by O_3 would then proceed to the point where it is "turned off" by decreased pH. The observed decrease in SO_2

(and O_3) would be a measure of the extent of the reaction. It should be pointed out that this experiment does not measure a rate constant for the reaction but only the net amount reacted. However Chameides and Stelson (1992) suggested that it is the flux of alkalinity that is important and not the rate. The rate is limited by the flux of sea-salt, not the rate of the reaction.

As discussed in Section IV the Calspan nebulizer is a good choice for introduction of the sea-water/aerosol into the chamber.

Results

The procedure tested was to inject about 120 ppb of O_3 into the chamber followed by about 30 to 50 ppb of SO_2. The wall losses for these two reactants were followed for about 20 minutes to establish a base line for wall losses. After about 20 minutes sea water nebulization commenced and continued until the SO_2 concentration dropped to about 10 ppb (typically 15 minutes). After nebulization ceased we continued to monitor SO_2 and O_3 concentrations to establish the wall loss baseline after the injection. Fig.39 shows the result for filtered (real) sea-water (from Aldrich). During these two runs 1.3 and 1.4 liters of seawater were used, respectively and the relative humidity was between 90 and 92%.

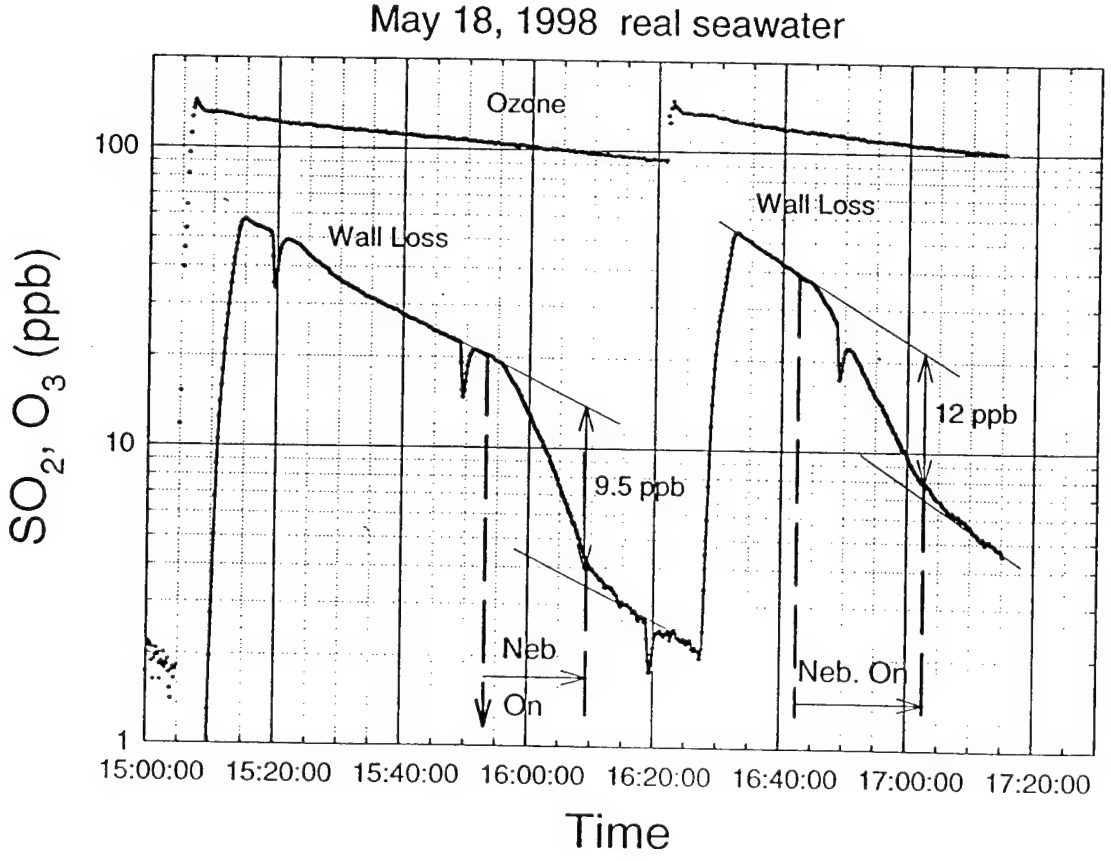

Fig. 39 – Loss of SO2 to sea-salt aerosol with ozone present

The amount of SO_2 consumed (after accounting for the wall loss) was about 9.5 and 12 ppb. The larger amount of SO_2 consumed in the second run may have been related to the larger SO_2 concentration during that run. It is clear from these results that while SO_2 was rapidly depleted by the sea-salt aerosol, no discernible depletion of O_3 was observed. This surprised us and so we repeated the experiment at the end of different experiment on the following day, after filtering to reduce the O_3 to below 3 ppb. Three consecutive runs were made; the latter two are shown in Fig. 40. Here the seawater injections were 1.15 liters in thirteen minutes and 1.10, also in 13 minutes. The SO_2 consumed were about 14.5 and 14 ppb, respectively, and the relative humidity 81% (80% increasing to 83%) and 84 % (82% increasing to 86%), respectively. It is also clear from the second day that ozone was not involved in the uptake of SO_2.

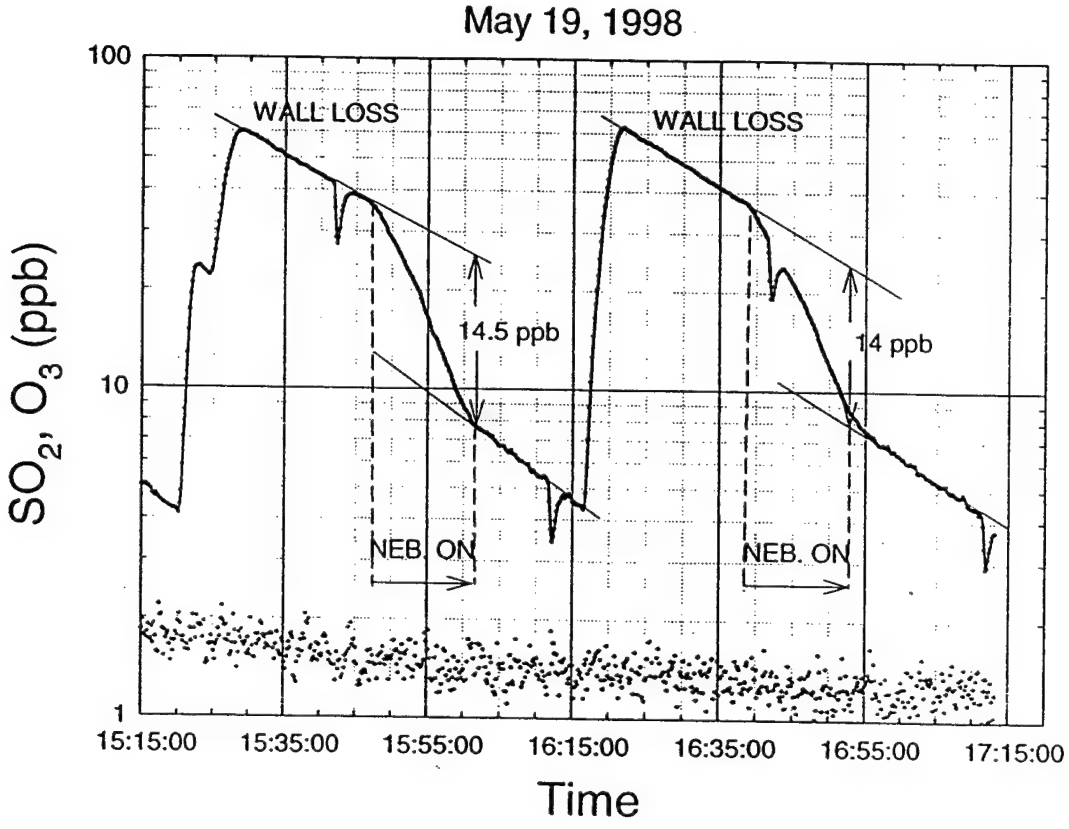

Fig. 40 – Loss of SO_2 to sea-salt aerosol with no ozone

The blips on the SO_2 trace are automatic zeros that occurred every half hour and were set to the minimum duration so as to minimize the disturbance of the trace. We later learned that this feature could have been disabled. (At this point the NRL TECO 42S had failed and Richard Leaitch of the Canadian Environmental Service graciously loaned a similar instrument to us. It had been modified for aircraft use and had the automatic zeroing capability that we did not need during our run because of the high concentrations employed.)

We also made a run with seawater generated from artificial sea salt obtained from Aldrich and found no observable uptake of SO_2. However in mixing the "seawater" solution we were unable, in the time available (several hours) to get some white residue in the salt to go into solution. This may have been the component that would have provided the buffering had we been able to get it into solution. The solution did have a pH of over 8 even without the residue being in solution.

The real sea water used in the experiment had been titrated with HCl and found to require $2.44X10^{-3}$ moles/liter to reach the equivalence point. This number agrees well with values given in the literature for seawater. One liter of seawater nebulized uniformly into the chamber would require a hydrogen equivalence of almost 90 ppb, or for SO_2 conversion to H_2SO_4 - 45 ppb of SO_2, to neutralize the alkalinity.

As a possible explanation of the observed SO_2 depletion without O_3 reaction, one should look into the enhanced uptake of S(IV) due to the alkalinity; i.e., greatly enhanced effective Henry's constant. We do not understand why the postulated O_3-SO_2 reaction did not take place. Possibly the acidity caused by S(IV) uptake in the high SO_2 environment turned this reaction off; in which case, our experiment may not be representative of the real atmosphere. Further study will need to be done to explain these observations.

Summary and Recommendations

1. It was demonstrated that we can measure the depletion of SO_2 in the chamber against the background of wall losses, and that under the conditions given, the depletion of SO_2 was not related to an SO_2 - O_3 reaction in the aerosol as originally expected.

2. We recommend that the investigators seriously consider whether or not they want to pursue heterogeneous reactions of SO_2 with sea-salt aerosol during the Fall set of experiments, in light of the following:

   (a) Repeating the above experiment will likely give the same result, and until we understand this result it will be difficult to design a better experiment.

   (b) Even if the experiment is successful, it is designed to give total uptake and not a rate, which would likely shed more light on the reaction.

   (c) We are undertaking more than we can probably do well. This would be one way to limit the scope of our investigations.

   (d) One of the investigators most interested in heterogeneous reactions may not be participating (due to funding difficulties) and therefore diagnostics of the reacted particles may be limited.

IX. UNIVERSITY OF WASHINGTON FILTER SAMPLING AND ION CHROMATOGRAPHIC ANALYSIS

The preliminary analysis of the filter samples taken by the University of Washington is shown in Table 4. The right hand column gives the conditions in the chamber. There are samples for the clean chamber (base-state) as well as samples for sulfate production in the dry chamber with SO_2 and ozone and after cloud processing for the ozone and H_2O_2 runs, and for cyclohexene and cyclopentene runs discussed earlier. Even though the mass loading in the chamber was sometimes only a few micrograms per cubic meter, enough mass can be collected from about one cubic meter of air to analyze.

Table 4 – Sampling Period: May 7th, 1998 to May 15th, 1998

Sample #	Sampling period (flow rate = 39 l/min unless otherwise indicated)	Gravimetric mass collected on front Teflon filter (μg)	Mass of anion species on front Teflon filter, calculated from IC analysis data (μg)	Calculated total mass density of aerosol ($\mu g/m^3$); *(possible components)*	Experimental condition --- what might be on the filter?
Cal1 (base-state3)	from 9:27am to 10:12am, May 7th; (45 min)	10	sulfate ~ 0	~ 0	background state --- clean chamber after filtering the chamber air overnight; no potential reactants injected.
Cal2 (blank2)	from 12:25pm to 12:35pm, May 7th. (10 min)	3	used to calculate noise level.		***blank sample*** --- with SO2 and O3 in the chamber; did not use pump.
Cal3 (sample5)	from 1:23pm to 1:53pm, May 7th; (30 min)	8	sulfate ~ 0.46	0.39 $\mu g/m^3$ (sulfate)	dark particle production and growth (with SO2 and O3 in the chamber).
Cal4 (sample4)	from 2:28pm to 3:48pm, May 7th, (80 min)	9	sulfate ~ 2.49	0.80 $\mu g/m^3$ (sulfate)	particle production and growth (with SO2 and O3 in the chamber) --- first 15 minutes lights on, then lights off.
Cal5 (sample3)	from 1:52pm to 2:52pm, May 8th; (60 min)	7	sulfate ~ 0.17	0.073 $\mu g/m^3$ (sulfate)	particle production and growth (initial O3 > 100ppb, SO2 > 10ppb); wet chamber (RH >80%); prepared for the formation of cloud #1.
Cal6 (sample4)	from 4:15pm to 4:38pm, May 8th; (23 min)	11	sulfate ~ 2.90	3.15 $\mu g/m^3$ (sulfate)	collecting aerosol sample from the chamber after the evaporation of cloud #1.
Cal7 (sample3) ***(Only Teflon filter was used.)***	from 1:08pm to 1:48pm, May 9th; at 50 l/min (40 min)	30	sulfate ~ 9.62	4.81 $\mu g/m^3$ (sulfate)	80ppb O3 and 20ppb SO2 were injected into the chamber initially. Then H2O2 was injected continuously for 2.5 hours before cloud #2 formed. Collected aerosol sample from the chamber after cloud #2's evaporation.

Cal8 (blank2)	from 12:08pm to 12:17pm, May 12th; (9 min)	11 (artifact?)	used to calculate noise level.		***Blank sample*** --- mass was exceptionally big for a blank sample, might be due to some artifacts on May 12th.
Cal9 (sample3)	from 2:01pm to 2:56pm, May 13th; (55 min)	23	glutarate ~ 0.093 succinate~ 0.097 sulfate ~ 0.152 oxalate ~ 0.089	0.201 $\mu g/m^3$ (sulfate, glutarate? succinate? oxalate??)	dark particle production and growth (with cyclohexene and O3 in the chamber).
Cal10 (sample3)	from 4:35pm to 5:00pm, May 13th; (25 min)	16	sulfate ~ 0.11	0.113 $\mu g/m^3$ (sulfate)	particle production and growth (SO2 was injected into the above chamber 0.5 hour after Cal9 sampling ended; lights on).
Cal11 (blank3)	from 8:50am to 9:00am, May 14th; (10 min)	6	used to calculate noise level		***blank sample*** --- clean chamber, some strange particles observed at the beginning of the day (due to the heater?).
Cal12 (sample1)	from 10:35am to 11:15am, May 14th; (40 min)	10	glutarate ~ 0.179	0.115 $\mu g/m^3$ (glutarate?)	dark particle formation and growth (with cyclopentene and O3 in the chamber); prepared for cloud #3's formation.
Cal13 (sample1)	from 5:10pm to 5:40pm, May 14th; (30 min)	19	glutarate ~ 0.290 sulfate ~ 0.066	0.304 $\mu g/m^3$ (glutarate? Sulfate??) The sulfate signal might be just noise.	collecting aerosol sample from the chamber after cloud #3's evaporation.
Cal14 (blank2)	from 11:40am to 11:55am, May 15th; (15 min)	1	used to calculate noise level.		***blank sample*** --- with SO2 and O3 in the chamber; did not use pump.

1. All the ***blank samples*** (2, 8, 11, 14) were taken when both Teflon-Quartz and Quartz-Quartz filter cassettes were connected to the chamber, but the pump was not used to suck the air (aerosol) out of the chamber as in other non-blank samples (1, 3, 4, 5, 6, 9, 10, 12, 13).

2. ***Flow rate*** was measured by the flow meter in the filtering apparatus.

3. ***Sampling period*** refers to the starting and ending time during which the pump was used to suck the aerosol out of the chamber at the corresponding flow rate.

4. All Teflon filters were measured gravimetrically before and after the sampling. The difference is shown in the table as ***gravimetric mass***.

5. Using peak heights or areas on a chromatogram and linear regression method, the mass (μg) of every detectable anion species was quantified. Furthermore, considering sampling volume, the mass density of aerosol in the chamber at the end of every run was also calculated and tabulated.

ACKNOWLEDMENTS

We thank John Callahan of NRL for analysis of background hydrocarbons. We also thank Richard Leaitch of the Atmospheric Environment Service of Canada for the loan of an SO_2 monitor. This work constitutes a contribution to the International Global Atmospheric Chemistry (IGAC) core project of the International Geosphere-Biosphere Programme (IGBP). Funding was provided by the National Ocean Partnership Program and also by the Office of Naval Research through the Naval Research Laboratory.

REFERENCES

Ambrusko and Wurster, 1991: Measurements of the Ashford Chamber Spectral Irradiance. Private communication.

Chameides, W. L. and A. W. Stelson, 1992: Aqueous-Phase Chemical Processes in Deliquescent Sea-Salt Aerosols: A Mechanism That Couples the Atmospheric Cycles of S and Sea Salt. *J. Geophys. Res.*, **97**, 20,565-20,580.

Chylek, P., 1978: Extinction and Liquid Water Content of Clouds. *J. Atmos. Sci.*, **34**, 296-300.

Hoppel, W. A., G. M. Frick, J. W. Fitzgerald, and B. J. Wattle, 1994: A Cloud Chamber Study of the Effect that Nonprecipitating Water Clouds Have on the Aerosol-Size Distribution. *Aerosol Sci. and Tech.*, **20,** 1-30.

Mackay, G. I., D.R. Karecki, and H.I. Schiff, 1996: Tunable Diode Laser Absorption Measurements of H_2O_2 and HCHO during the Mauna Loa Observatory Photochemistry Experiment. *J. Geophys. Res.*, **D101**, 14,721-14,728.

Seinfeld, John H. and Spyros N. Pandis, 1998: *Atmospheric Chemistry and Physics* (John Wiley and Sons, Inc., New York).

Stedman, D. H. and Hiromi Niki, 1973: Photolysis of Nitrogen Dioxide in Air as Measurement Method for Light Intensity. *Environ. Sic. Technol.*, **7**, 735-9.

APPENDIX A

Hydrocarbon Measurements

Measurements of gas phase hydrocarbon compounds in the chamber during the Phase 1 experiments were performed by Calspan employing both GC and GC-MS in conjunction with thermal desorption. These instruments were used to qualitatively identify background hydrocarbons in the chamber and to quantify the monitored hydrocarbons for wall loss rates and ozone reactions during the baseline Phase 1 experiments.

Analytical Instrumentation

The gas chromatograph (GC) used was a Hewlett-Packard model 5890 Series II+ equipped with a flame ionization detector (FID). The GC was controlled with the HP-Chemstation for PC software using the HP-IB interface. No gas flow was set at the injector inlet, since carrier gas flow came through the Dynatherm ACEM900 flow controller. The GC column was a Supelco Petrocol-DH capillary column, 100 meters by 0.25 mm. The FID was operated at a temperature of 250 °C with a hydrogen flow of 17 cc/min and an air flow of 405 cc/min. Some of the testing used an auxiliary gas flow of nitrogen at 11 cc/min, but that was discontinued since it caused the FID flame to go out occasionally and did not change the sensitivity of the analyses. Manual integration was only used rarely as needed, though integration parameters were occasionally changed to maintain a reasonable baseline and obtain a reasonable number of peaks integrated.

The mass spectrometer is a Discovery2 quadrupole ion trap unit from Teledyne Electronic Technologies Inc. The mass spectrometer was directly connected to the outlet of the GC column. The characterization was done using straight electron impact ionization.

Sampling and Analytical Protocol

Thermal desorption of collected samples were performed using a Dynatherm ACEM900 single tube thermal desorption unit. The unit was coupled directly to the GC column through a length of fused silica capillary fed through a heated (250 °C) tube that entered the GC oven. The unit was used with either Tenax-TA thermal desorption sample tubes in conjunction with a Tenax-TA focussing trap, or with Carbotrap-300 thermal desorption sample tubes in conjunction with a Carbotrap-201 focussing trap depending upon the application. Nitrogen was used as the purge gas for the sorbent tubes as well as the carrier gas through the focussing trap to the GC. Nitrogen flow through the sorbent tubes was set at ~25 cc/min, while nitrogen flow to the GC was set at ~1 cc/min. Specific analytical conditions were documented separately for each experiment, but in general, the following conditions were used:

	Tenax-TA	Carbotrap-300
Dry time	1 min	1 min
Tube heating time	5 min	5 min
Tube Temp (°C)	280	350
Cool time	2 min	2 min
Trap heating time	2 min	2 min
Trap Temp (°C)	310	375

Sorbent tubes were recycled by conditioning them using the Dynatherm single tube conditioning unit. Sorbent tubes were conditioned for 10 min at a temperature close to the maximum with nitrogen flowing through the tube at ~50 cc/min. Tubes were allowed to cool with nitrogen flowing, and then were put into capped glass storage tubes.

Experimental Results

Results of the various analytical runs will be presented in separate sections. Each section will contain a brief description of the experiment and any pertinent information along with calibration data and final results.

Cyclohexene Wall Loss Experiment

On May 13, 1998 the chamber was challenged with 50 ppb cyclohexene in order to determine wall losses. The chamber air was sampled using duplicate Tenax-TA sorbent tubes at half-hour increments starting at t=0 through t=2 hr and also twice during the ozone reaction period. All of the wall loss samples were sampled for 15 min each at 150 cc/min; the first ozone sample overran at 87 min and the second ran for 15 min. The sorbent tubes were analyzed as described in the Instrumental Setup section. The 1.5 hr sample gave lower results, so the backup tube was run giving reasonable results. It is necessary that the calibration work be carried out on another day due to the time required to run the samples and turn around tubes for re-use.

On May 15, three sorbent tubes were prepared and run for calibration purposes using 10, 20, and 40 µL of the 4170 ppm cyclohexene gas mix. The results, while linear, did not appear to be totally satisfactory. On May 21, two sorbent tubes were prepared and run using 20 and 50 µL of the 4170 ppm cyclohexene mix. This second set appeared to be much more satisfactory and agreed well with the 40 µL sample run on 5/15. It was decided to use these results as a calibration for the wall loss run; and in particular to use the results obtained by peak area since that calibration gave the lowest intercept value.

Some difference(s) in sampling technique is suspected for the difference in the calibration curves. The 5/21 curves are preferred because of linearity of response, and lower intercept values. Note that it is expected that the larger errors in sampling should be found with the smallest volumes. The sampling errors are expected to come from the syringe transfer of sample to the sorbent tubes and are not an issue with the actual air samples taken from the chamber. Cyclohexene calibration data follows:

Date	Sample (µL)	Ret. Time	Area	Peak ht.
05/15/98	10	20.127	544407	47007
	20	20.212	705205	55240
	40	20.177	880124	74436
05/21/98	50	21.564	1167601	85361
	30	21.457	717918	56791
5/15			r=0.986	r=0.999
			m=8.97e-5	m=1.085e-3
			b=-40.4	b=-40.5
5/21			m=4.45e-5	m=7.00e-4
			b=-1.93	b=-9.76

The calculated analytical results for the wall loss samples, as well as the ozone reaction sample are given in Table A1. Wall loss values are shown in Fig. 15 in the text. Results are calculated as the µL equivalent of the standard gas mix (4170 ppm) that was used both to challenge the chamber (by dilution) and to provide the instrumental calibration. By dividing that number by the volume sampled (in µL) we get the fraction of standard gas in the chamber. Multiplying the fraction by the concentration of the gas in ppb gives the concentration of cyclohexene in the atmosphere sampled.

Table A1 – Cyclohexene Analytical Results for Wall Losses

Sample (hr)	Ret. time	Area	Results (μL)	Vol. (mL)	ppb
t=0 (backup)	20.208	610772	25.2	2250	47
t=0	20.082	609507	25.2	2250	47
t=0.5	20.159	602550	24.9	2250	46
t=1	20.182	585111	24.1	2250	45
t=1.5	20.284	453534	18.2	2250	34
t=1.5 (backup)	20.440	579505	23.8	2250	44
t=2	20.252	601836	24.8	2250	46
Ozone (15 min)	20.306*	361183	14.1	2250	26

* Double peak; 19.993 was the ret. time for the other half. Area and peak heights were of the same order of magnitude for both. The 87 min. ozone sample also showed a double peak.

Alpha-pinene Wall Loss Experiment

On May 19, 1998 the chamber was challenged with 10 ppb alpha-pinene in order to determine wall losses. The chamber air was sampled using Tenax-TA sorbent tubes at half-hour increments starting at t=0 through t=2 hr and also during the ozone reaction period. The t=0, t=1, and t=2 hr samples were taken in duplicate. Two samples of the ozone reaction were taken consecutively for 20 min each. The sorbent tubes were analyzed as described in the Instrumental Setup section. The alpha-pinene standard gas samples were also run at 500, 250, and 100 μL of the 174 ppm alpha-pinene gas mix.

A two point calibration was decided upon for alpha-pinene, just as was the case for cyclohexene. While the 50 and 250 μL samples appear linear, the 100 μL sample looks out of line. If the 100 μL sample is eliminated, it would calculate back as 143 μL and the y-intercepts would drop to –70.5 and –63.7 for area and peak height, respectively. The two point peak height curve is best used. The results are as follows:

Date	Sample (μL)	Ret. Time	Area	Peak ht.
05/19/98	500	26.353	427253	80804
	250	26.362	240014	44970
	100	26.389	159911	29663
			r=0.9965	r=0.9964
			m=1.468e-3	m=7.67e-3
			b=-121.3	b=-114.1
2 point:			m=1.335e-3	m=6.977e-3
			b=-70.5	b=-63.7

The calculated analytical results for the wall loss samples, as well as the ozone reaction sample are given in Table A2. Wall loss values are plotted in Fig. 16 in the text. Results are calculated as the μL equivalent of the standard gas mix (174 ppm) that was used both to challenge the chamber (by dilution) and to provide the instrumental calibration. By dividing that number by the volume sampled (in μL) we get the fraction of standard gas in the chamber. Multiplying the fraction by the concentration of the gas in ppb gives the concentration of alpha-pinene in the atmosphere sampled.

Table A2 – Alpha-Pinene Analytical Results for Wall Losses

Sample (hr)	Ret. time	Area	Results (µL)	Vol. (mL)	ppb
t=0	26.480	25871	116.8	2250	9.0
t=0.5	26.326	28662	136.3	2250	10.5
t=1	26.365	27172	125.9	2250	9.7
t=1.5	26.391	30244	147.3	2250	11.4
t=2	26.373	24949	110.4	2250	8.5
Ozone prod.#1	26.498	18059	62.3	3000	3.6

Dimethyl sulfide Wall Loss Experiment

On May 20, 1998 the chamber was challenged with 30 ppb dimethyl sulfide (DMS) in order to determine wall losses. The chamber air was sampled using Carbotrap-300 sorbent tubes at half-hour increments starting at t=0 through t=2 hr. and also during the ozone reaction period. None of the samples were taken in duplicate, except for the ozone reaction samples. The two samples of the ozone reaction were taken consecutively for 20 min each, while all of the others were sampled for 15 min each. The sorbent tubes were analyzed as described in the Instrumental Setup section. The DMS standard gas samples were also run at 5, 10 and 15 µL of the 5260 ppm DMS gas mix.

The DMS peaks appeared a little broad but gave a good linear regression for both area and peak height. The regression was better, however for the peak heights. Peak height results should probably be used even though the differences are small. Intercepts in both cases were quite low. The results are as follows:

Date	Sample (µL)	Ret. Time	Peak ht.
05/20/98	5	18.535	4851
	10	18.549	9433
	15	18.577	13999

r=0.9999
m=1.093e-3
b=-0.31

The calculated analytical results for the wall loss samples, as well as the ozone reaction sample are given in Table A3. Wall loss values are plotted in Fig. 17 in the text. Results are calculated as the µL equivalent of the standard gas mix (5260 ppm) that was used both to challenge the chamber (by dilution) and to provide the instrumental calibration. By dividing that number by the volume sampled (in µL) we get the fraction of standard gas in the chamber. Multiplying the fraction by the concentration of the gas in ppb gives the concentration of dimethyl sulfide in the atmosphere sampled.

Table A3 – Dimethyl Sulfide Analytical Results for Wall Losses

Sample (hr)	Ret. time	Peak height	Results (μL)	Vol. (mL)	ppb
t=0	18.604	11040	11.8	2175	28.4
t=0.5	18.488	8771	9.3	2175	22.4
t=1	18.429	9419	10.0	2175	24.1
t=1.5	18.505	8048	8.5	2175	20.5
t=2	18.429	10015	10.6	2175	25.7
Ozone prod.#1	18.465	13075	14.0	2900	25.4